DYNAMIC CORTICAL MECHANOTRANSDUCTION DRIVES ROUNDED CELL PROTRUSIONS

J.Nancy Costigliola

A dissertation submitted to the faculty of the University of North Carolina at Chapel Hill in partial fulfillment of the requirements for the degree of Doctor of Philosophy in the Department of Cell and Developmental Biology

Chapel Hill
2012

Approved by:

Ken Jacobson, PhD

Tim Elston, PhD

Keith Burridge, PhD

James Bear, PhD

Jason Haugh, PhD

Abstract

J.NANCY COSTIGLIOLA: Dynamic cortical mechanotransduction drives rounded cell protrusions
(Under the direction of Ken Jacobson, PhD)

As cells decrease their area of attachment, as occurs in 3D migration, F-actin is remodeled from integrin-dependent, relatively flat networks to a contractile cortex located at the rounded cell periphery. Concurrently, as the area of attachment decreases, dependence on myosin II contractility for cell motility increases (Doyle et al., 2009; Friedl and Wolf, 2010). I investigated the dynamic behavior and regulation of actomyosin-driven periodic protrusions in rounded fibroblast and endothelial cells. Because this contractile behavior is periodic, the regulation of the contractility must be due to negative and, possibly also positive, feedbacks. To that end I investigated two major regulatory pathways of myosin II contractility, Calcium and the small GTPase RhoA. Although Calcium is known to govern periodic contractility and signaling in other systems (Berchtold et al., 2000; Chen et al., 2009; Katz and Repke, 1966; Kruskal and Maxfield, 1987; Lee et al., 1999; Marks and Maxfield, 1990; Somlyo and Somlyo, 2003)and had been previously implicated in our system by both theoretical and experimental evidence(Kapustina et al., 2008; Pletjushkina et al., 2001; Salbreux et al., 2007; Weinreb et al., 2006; Weinreb et al., 2009), I found no evidence of periodic calcium release governing myosin activity in these protrusions. Rather, I found that RhoA activity exhibited spatiotemporal oscillatory behavior. RhoA activity, co-localized

with the actin cortex, traveled in waves, and was necessary for periodic protrusions. By investigating the regulation of these waves, I found evidence that the waves are regulated by a positive feedback loop at the cortex from myosin II, which is downstream of RhoA, to GEFH1, which is upstream of RhoA. Further, this positive feedback of the RhoA pathway reveals a novel form of cortical mechanotransduction that occurs independently of integrin-mediated signaling, a property that could be useful for cells migrating with reduced substrate affinity in 3D environments.

Dedication

I dedicate this work to my husband Joshua Tarsky, my daughter Aviva Tarsky, and to all my friends, family, and colleagues that have helped us extensively throughout my time in Chapel Hill.

Acknowledgements

Ken Jacobson and my colleagues in his laboratory have been instrumental in my personal and scientific development as a doctoral student. The lab has always been a creative environment with diverse interests and room for exploration. Ken has given us free reign in our research, an approach that has been essential in developing an ability to effectively communicate my work and to plan research independently. I thank Ken for his devotion to his students and to interesting science, for the independence given, for his generosity with his time and contacts, and for his help in securing me a postdoctoral position. I thank Gabriel Weinreb for his time as my mentor and for his lasting contribution that the work should be fun; Maryna Kapustina for her time, effort, and patience as a colleague, mentor, and friend; and Michelle Itano and Zaozao Chen for their support and camaraderie.

Also, essential to my development and encouraged by the Jacobson lab, have been my collaborations with other labs at the University. These collaborations have been essential to the development of my project and progress as a scientist. I thank these collaborators specifically in the Chapters that follow. I thank my committee members for their support during and outside of committee meetings; Tim Elston, my co-mentor, for his sharpness and analytical perspective essential to the work; Keith Burridge, for his unending patience throughout my graduate work, his general advice and open-door policy; Jim Bear for his advice both scientific and professional; and Jason Haugh for his

valuable experimental and theoretical expertise as well as his extensive travel time on route 40. I thank the NIH Cell Migration Consortium GM64346 for creating an outstanding learning environment in which students and post-docs received valuable feedback on their individual research from senior researchers. I thank Barry Lentz and the UNC Biophysics for funding me on the Biophysics Training Grant and for my exposure to quantitative biology. I also thank the American Heart Association for providing me with two years of stipend and travel funding (09PRE2220021).

Finally, I would also like to express gratitude towards the Oscillating Cell itself. It has been a unique and trying companion as we have tried and are, I think, finally succeeding in discovering some of Its secrets. I hope that our work will inspire others to study this useful model system of cortical protrusions.

Preface

The work shown in Chapter Two was succedent to 4 papers (Kapustina et al., 2008; Pletjushkina et al., 2001; Weinreb et al., 2006; Weinreb et al., 2009) by our group and 1 paper by an outside group (Salbreux et al., 2007) implicating calcium as the oscillating regulatory factor in periodic protrusions. I found that cells could oscillate in the absence of calcium sources and did not detect any whole cell or local oscillations via calcium probe imaging. I also found that cells protrude periodically (oscillate) in the absence of reagent based MT depolymerization. In Ch.4 I show evidence that MT depolymerization occurs upon cell rounding. Based on my work, I believe that MT depolymerization, due to both its structural and biochemical effects, is the limiting factor in allowing a rounded fibroblast or endothelial cell to protrude with detectible peridiocity and amplitude. I performed the work in Chapter Two (Figures 2.1-2.6) in co-authorship with Maryna Kapustina, who provided the work shown in Figures 2.5, 2.7-2.8, and with assistance from all co-authors.

The work shown in Chapter Three would not have been possible without my collaboration with Richard Allen, who wrote the analyses programs for Figures 3.1 and 3.2 (see Methods), and Christophe Guilluy who performed the GEF activity assays in Figure 3.3.

Table of Contents

List of Figures

Abbreviations/Glossary

RhoA-Ras homolog gene family member A

1D-1 dimensional

2D-2 dimensional

3D-3 dimensional

MT-microtubules

ROCK-Rho kinase

GFP-green fluorescent protein

RFP-red fluorescent protein

CFP-cyan fluorescent protein

ERM-ezrin, radixin moesin family of proteins

FAK-focal adhesion kinase

CD44-cell surface glycoprotein

PSGL-1- p-selectin glycoprotein 1

PKA- protein kinase A

MTOC-micotrubule organizing center

p-MLC-phosphorylated myosin light chain

GTPase-hydrolase enzyme specific to guanosine triphosphate (GTP)

Rac- a subfamily of the RhoGTPases

Cdc42-cell division control protein homolog 42, a member of the RhoGTPase family

ICAM-1-intercellular adhesion molecule 1

VCAM-1-vascular cell adhesion molecule 1

FA- focal adhesion

Erk-extracellular signal related kinases

Src-tyrosine kinase named after the sarcoma virus

Fyn-tyrosine kinase

LARG- Rho guanine nucleotide exchange factor 12

GEFH1-Rho guanine nucleotide exchange factor 2

p115-Rho guanine nucleotide exchange factor 1

F-actin-filamentous actin

SEM-scanning electron micrograph

TEM-transmission electron micrograph

FFT-fast fourier transform

ER-endoplasmic reticulum

ATPase-enzyme that catalyzes dephosphorylation of adenosine triphosphate

EGTA-ethylene glycol tetraacetic acid

RhoGAP-GTPase activating protein

ODE-ordinary differential equations

PM-plasma membrane

DIC-differential interference contrast

ABP-actin binding proteins

PMT-plasma membrane target

CHO-chinese hamster ovary cell

RBD-Rho binding domain

GST-glutathione S-transferase

siRNA-short interfering RNA (ribonucleic acid)

RGD-arginyl-glycyl-aspartic acid peptide

CHAPTER 1

INTRODUCTION

Periodic protrusions of the actomyosin cortex provide a model for studying cortex-based motility. Much of what we know about the regulation and structure of migrating cells is based on studies performed on homogeneous two-dimensional surfaces. In contrast, *in vivo* extracellular environments consist of tissues with varied compositions and topographies. Cells migrating in 3-dimensional environments adopt rounder morphologies and significantly decreased substrate attachment compared to those moving on planar surfaces (Doyle et al., 2009; Friedl and Wolf, 2010). However, the difficulty of imaging with sufficient spatiotemporal resolution in 4-dimensions (through the 3D environment and over time) has limited our understanding of *in vivo* migration. Further, the study of migration in live animals and the design of artificial 3D substrates presents technical Catch-22s (Hakkinen et al., 2011; Legant et al., 2009; Raghavan et al., 2010): if 3D matrices are made non-uniform as they are *in vivo* it is difficult to study their mechanical properties; if they are uniform they do not recapitulate the *in vivo* environment. Here, we present studies of fibroblast and epithelial cells that have been detached from the substrate and which subsequently exhibit periodic protrusions in 3-dimensions. These rounded cell protrusions have allowed us to examine dynamic regulation of the cytoskeleton

independently of substrate composition and architecture. Further, because these protrusions are periodic they provide unique quantitative insight into the mechanochemical regulation governing the rounded cell cytoskeleton.

A Brief History of Periodic Protrusion Studies. Periodic protrusions were first observed in human lymphoblasts with depolymerized microtubules (MTs) in 1989 (Bornens et al., 1989). The phenomenon involved a constriction ring containing myosin II that dynamically opposed the site of "membrane protrusion." In 2001, our lab found that (Pletjushkina et al., 2001) spreading fibroblast and epithelial cells with depolymerized MTs also underwent periodic protrusions. These protrusions were dependent on myosin II phosphorylation, actin polymerization, and Rho-kinase activity. They also appeared to undergo out-of-phase oscillations in total cell calcium levels as evidenced by calcium probe imaging. Later, the Sykes group used confocal microscopy to image lymphoblasts and fibroblasts expressing actin-GFP and myosin-GFP and in which MTs had been depolymerized (Paluch et al., 2005). From this study, it appeared that no actin or myosin initially entered the protrusion. Although no membrane probe was used in this study, it became widely interpreted (Charras and Paluch, 2008; Fackler and Grosse, 2008; Friedl and Wolf, 2010) as employing membrane protrusions free of actin, or "blebs."

What is "blebbing?"The medical definition of a bleb is a "large blister filled with serous fluid" (Jain, 2005)and provides the basis for the current cell biology usage. In 1973 Fundulus blastula cells were described as undergoing "blebbing" undulations that increased in amplitude over time and led to lobo- and lamelli- podia

during mid-blastula stage migration (Tickle and Trinkaus, 1973; Trinkaus, 1973). Importantly, these studies demonstrated that rounded cell protrusions during development were associated with migration. However, as the authors themselves note, experiments were done at very low resolution. Charras and Mitchison have published the highest resolution images of bleb formation outside of any motility context, see Fig 1.1. (Charras et al., 2008; Charras et al., 2006).

Fig 1.1 : Ezrin (an ERM protein) in green and actin in red. The membrane protrudes with no visible actin cortex, indicating detachment from the central cortex shell. At 30 s actin is present at the cortex. The authors' interpretation is that ERM proteins provide a scaffold at the membrane edge to which actin can bind and polymerize. Inset at 42 s is magnification of this frame. Confocal sections with 100x magnification, bar is 2μm (Charras et al., 2006).

Fig 1.1

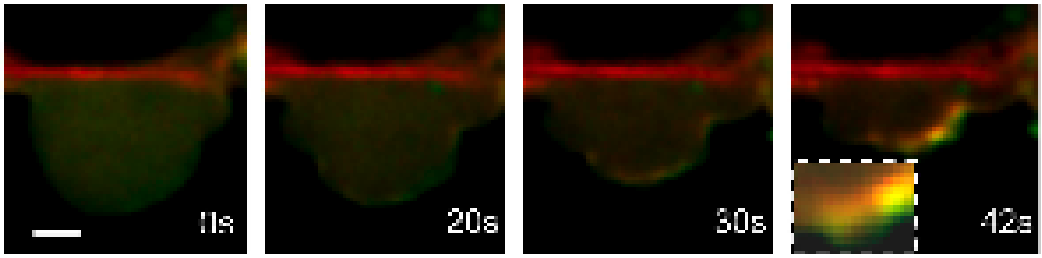

This research was originally published in Journal of Cell Biology. Charras GT, Hu CK, Coughlin M, Mitchison TJ. Reassembly of contractile actin cortex in cell blebs. *Journal of Cell Biology*. 2006; 175(3):477-90. © The Rockefeller University Press.

Their work has provided the current definition of blebbing:

> Bleb nucleation is initiated by the rapid detachment of a patch of membrane from the cortex…When expansion stops, contractile cortex reassembles under the bleb membrane, and the bleb is retracted. (Charras et al., 2006)

According to this definition, a bleb involves a break in the central actin cortex in which a membrane protrusion escapes due to cytosolic pressure. No actin reassembles at the bleb edge until the bleb has reached its maximum size.

Charras (Charras et al., 2006) provides evidence for small blebbing protrusions in non-motile cells. However, as Harrill and Martinac note, the membrane bilayer cannot expand or retain a stable shape when subject to environmental forces (Hamill and Martinac, 2001). This by necessity would limit any possible bleb involvement in migration to very soft substrates such as in zebrafish development (Blaser et al., 2006; Diz-Munoz et al., 2010) and/or to peripheral roles in cell advancement (Cunningham et al., 1992; Lorentzen et al., 2011).

Lobopodia-type protrusions, which are short and blunt, are accomplished via actomyosin contractility in many cancer and embryonic cells(Friedl and Wolf, 2010; Sahai and Marshall, 2003). However the term "blebby amoeboid movement" has come to describe rounded cell movement of nearly all types other than leukocytes (which have a clearly identified alternate migration mechanism of filopodia at the leading edge). This trend has occurred independently of data demonstrating actin cortex detachment from the membrane for a given cell type. Reviews (Charras and Paluch, 2008; Fackler and Grosse, 2008; Friedl and Wolf, 2010) on rounded cell

migration consistently refer to the original work in periodic protrusions (Paluch et al., 2005)as support for amoeboid blebbing during migration. Figure 1.2 is from a 2008 Nature Molecular Biology Review (Charras and Paluch, 2008) suggesting that the rounded cell periodic protrusions (1.2 D), free of actin cortex, provide the protrusive mechanism for rounded cell 3D migration (1.2 E).

Fig 1.2 (A) A tumour cell, in blue, migrating through a collagen matrix. Estimated point of contraction shown by arrows in the first three images. Protrusion direction shown in the last image on the right. Time between images 7 min. Scale bar, 20 μm. Reproduced, with permission, from the original publication of Wolf, Mazo 2003. (B) "Bleb" migration of a deep cell in a mid-blastula fish embryo. The authors interpret the image as exhibiting actin cortex detachment from the membrane. The protrusion broadens before elongating into a lobopodium in the last image on the right. Time between images is 4 s. Scale bar, 50 μm. Reproduced, with permission, from the original publication of Kageyama T. 1977. (C-E) Schematics of protrusions the authors interpret as blebbing, in which the leading edge prior to blebbing is indicated by a dotted line. (C) Schematic of 2D periodic protrusions with attachments indicated by pink dots. (D) Schematic of periodic protrusions between two glass coverslips. (E) 3D matrix movement.

Fig 1.2

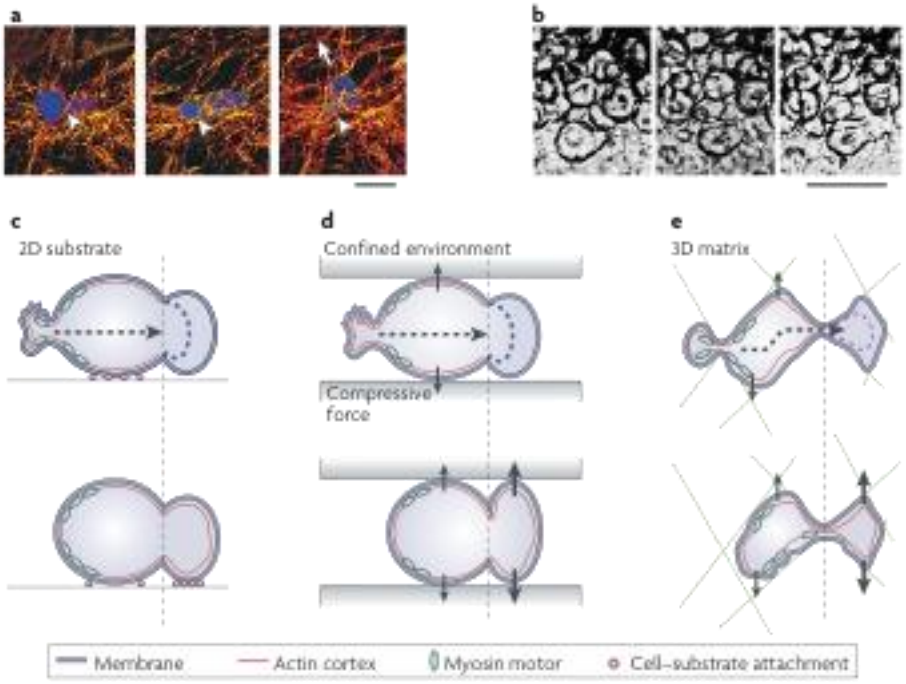

Reprinted by permission from Macmillan Publishers Ltd: [NATURE REVIEWS MOLECULAR CELL BIOLOGY] Charras G, Paluch E. Blebs lead the way: how to migrate without lamellipodia. *Nature Reviews Molecular Cell Biology* 9(9) 730-6), 2008.

However, blebs occur with rapid expansion (30s) but slower retraction (2 min) (Charras et al., 2008), than do rounded cell protrusions, which occur periodically, with equal protrusion and retraction times (Costigliola et al. 2010). Further, investigation of the membrane-cortex association during periodic protrusions had not yet been done, leading one to question the association of the two during periodic protrusions. In fact, Maryna Kapustina in our group carried out a number of experiments to determine the role of blebbing in periodic protrusions. A summary of this work is presented in the following section.

An alternative to blebbing: accordion-like folding of the membrane-cortex interface Rounded cell periodic protrusions are regulated in part by a traveling wave of contractility within the cortex exhibiting positive feedback from myosin II contractility to RhoA (see Chapter 3). To investigate the structure of the cortex during this dynamically regulated contractility and subsequent protrusions, we used CHO cells that stably express the 17-amino-acid peptide, Lifeact, fused to GFP; which labels filamentous actin (F-actin) structures in eukaryotic cells and tissues (Riedl et al., 2008). Periodic protrusions are amplified by microtubule depolymerization (Costigliola et al. 2010), which we employ unless otherwise noted, making them easily observed and quantified by standard microscopy techniques. Time-lapse imaging using DIC and epifluorescence shows how the morphology and actin cortex concurrently change during peroiodic protrusions (Fig. 1.3 A). Fig. 1.3 B presents one complete period of the oscillatory phenotype and demonstrates the location and density of the highly polarized F-actin (green) and myosin (red)

containing cortex. Note the striking similarity in the F-actin and myosin distributions at the beginning (t=0) and at the end of the period (t=65s). This highly periodic behavior often repeats for several hours, demonstrating that the protrusions are a mechanochemically regulated process and not driven by stochastic fluctuations.

Fig 1.3 Actin and the membrane co-localize throughout the protrusion cycle. Cytoskeletal and membrane dynamics and coordination during periodic protrusions. A. DIC and Lifeact-GFP wide field fluorescent images of an oscillating cell. B. Cytoskeletal dynamics during one period of oscillation. Fluorescence image of f-actin (green) and myosin (red). The highest densities of cortical F-actin correlate with active myosin (Costigliola et al. 2010) and remain highly polarized throughout the oscillatory cycle. (C-E) C. Predictions of fluorescent signal outcome based on two different models for the rounded protrusions: (I) the PM bleb model (Paluch et al., 2005); (II) the dynamic cortex-membrane couple model (see text). Schematic drawing presents cell top view (left panel) and plot of fluorescent signals within the rectangle (right panel) of cortical F-actin (green) and plasma membrane (red) D. Time-lapse of confocal fluorescent images of CHO cells stably transfected by Lifeact-EGF (green) and transiently transfected with PMT-mRFP (membrane marker, red). The yellow rectangles show the positions where the fluorescent signal was analyzed. To the right of the images, plots of the averaged line scans of fluorescence intensity going from the left to the right of the cell. E. Correlation plot between maximum intensity of F-actin (GFP-Lifeact) and plasma membrane marker fluorescence at the cell periphery. 20 consecutive frames were used for analysis . Each frame provides two positions for correlation analysis where the rectangle intersects the cell margin; the arrows in D (top right panel) denote examples of chosen positions (vertical arrows, cortex; oblique arrows, membrane). Correlation

coefficient for two fluorescent intensities is R=0.95. Scale bars in A and B are 5μm; time is in seconds. This figure was provided by Maryna Kapustina.

Fig 1.3

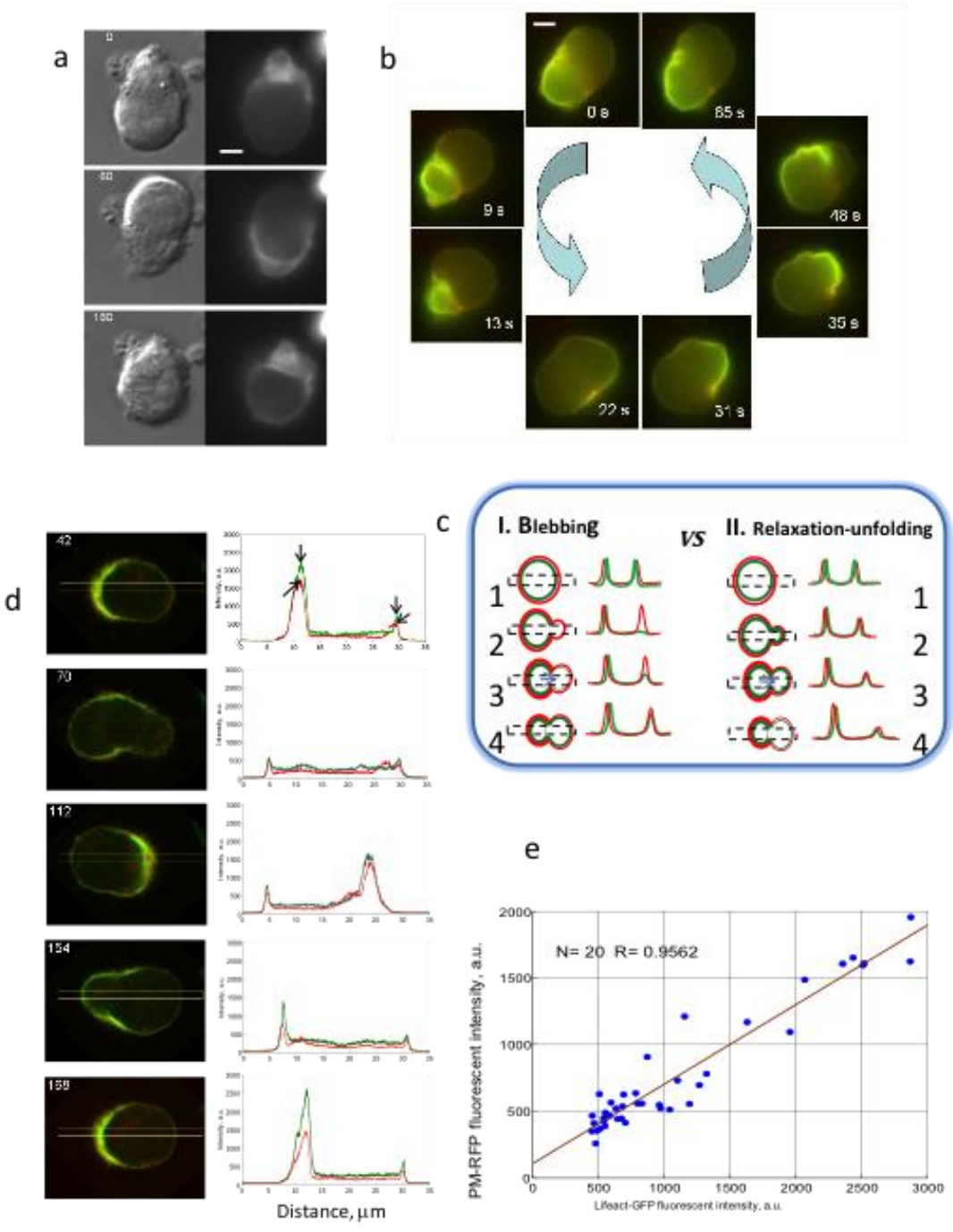

Figure 1

We used high-resolution microscopy to investigate the claim that periodic protrusions of rounded cells occur via membrane blebbing. In Figure 1.3 C we provide a schematic for the expected fluorescence signal distributions of protrusions driven by blebbing. The resting, rounded cell, at its periphery, should show similar values for the cortex and membrane, respectively, at any azimuth within a narrow rectangle placed on the cell. During blebbing, when the PM detaches from the cortex and expands, the membrane signal would be visible without the corresponding cortical F-actin signal. When the cortex redevelops to support the bleb, a weak F-actin signal would re-appear. During the period of the protrusion cycle, the F-actin signal would grow as the protrusion expands until the developing cortex becomes strong enough to resist cytosol pressure thereby preventing further expansion. Eventually cortical development would be complete as the F-actin signal returned to its initial value.

What we find and describe in this paper, however, is that the membrane and cortex simultaneously undergo coordinated shape changes so that the membrane is supported by at least a thin F-actin-containing cortex at all times, see Fig 1.3 C and D. Therefore, there are qualitative differences between what we observe and what would be seen in a blebbing phenotype. Signals from F-actin and the PM become progressively weaker during protrusion growth and stronger as the protrusion retracts. In all stages of protrusion the membrane and F-actin signals were highly correlated (Fig. 1.3 E). The plasma membrane has a limited capacity for areal extension (less than 4%) before rupture (Sheetz et al., 2006) but a high degree of plasticity with a low

bending energy (Farsad and De Camilli, 2003; Lipowsky, 1991) which make it a good candidate for folding. In contrast, the supporting cortex is a highly dynamic structure in which myosin and actin binding proteins determine the network architecture and allow for a variety of cell shapes.

There is a strong correlation between cortical actin and membrane signals during periodic protrusions (Fig. 1.3 E and D). When the PM on one side of the cell has protruded and the image shows apparent "thinning" of the PM, the underlying cortex also appears thinner. This behavior is quantified using a scatter plot (Fig. 3.1 E) of cortical F-actin fluorescence versus plasma membrane fluorescence signals from the same location on the cell border. These two signals are strongly correlated with an average correlation coefficient of $R=0.87\pm0.078$ for 22 cells from 10 different experiments. It is also important to note that a decrease in fluorescent signal is correlated with the protrusion expansion and increase of signal corresponds to the protrusion retraction (compare Fig. 1.3 D 70 vs 112 s). The thickness of the membrane and cortex on the cell periphery estimated from these signals are also highly correlated.

Accordion-like folding. We also analyzed the surface area of cells in the spread and rounded states. During cell rounding, the apparent surface area of the cell decreases by up to 6 fold requiring the surface to be compacted in less than 1 minute. On this time scale, folding of the membrane must be the predominant process as opposed to endocytosis. Indeed, the plasma membrane after cell rounding is highly convoluted (Costigliola et al. 2010). Because in the spread cell the plasma membrane

is supported with thin layer of underlying cortex between 50 and 200nm thick (Pesen and Hoh, 2005), it is possible that during rounding the underlying cortex does not detach but folds with the membrane. As the protrusion develops, the membrane-cortex layer unfolds to provide the additional cell surface required to cover the protrusion (see Fig 1.4).

The presence of folds on the periphery of cells undergoing periodic protrusions was confirmed by transmission electron microscopy (Fig 1.4 A). Note that one region of the cell margin shows folds that appear as closed compartments in the thin section while the distal regions of the cell appears smooth corresponding to the protruding region. The amplitude of the folds varied from 50nm to nearly 2μm. The region of densely compacted folds correlates with the position of denser material (arrows), presumably the underlying cortex. The majority of small folds cannot be visualized by traditional optical methods because of their density and size. When folds are compressed and dense, they appear in the image as a thick and wide band on the cell margin. When the cortex relaxes and releases highly compacted folds, they become more visible in the optical section.

Our data indicates that a coupled membrane-cortex contraction dilation mechanism drives rounded cell periodic protrusions, as depicted in Fig. 1.4 C (center panel). The PM and cortex remain coupled in all phases of periodic dynamic protrusions and these protrusions occur via an unfolding of the membrane-cortex composite layer. In the first frame (t=7s), the image depicts the situation when the membrane and cortex have a dense and compact structure (width ~1.7 μm) that

originates from membrane-cortex folds as described schematically in the center panel (top). We assume these folds are kept intact by the underneath actin-myosin network (Cai et al., 2010)which is crosslinked by actin binding proteins (ABPs) (Carreno et al., 2008; Doherty and McMahon, 2008; Nambiar et al., 2009). When the activity of myosin and ABPs decreases, the folds are released and the membrane-cortex couple relaxes and dilates due to cytosolic pressure. An image in the same location at a later time (42 s) shows a substantially thinner membrane-cortex coupled layer with decreased intensity. At later times (t=77s), the membrane and cortex are fully dilated, having an apparent width of ~0.3 μm. Following this stage, the process of contraction and folding occurs bringing the cell margin back to its initial state (t=119s) in which the cortex and membrane signal are both wider and more intense. The relaxation and releasing of the folded cortex-membrane creates a traveling wave wherein contractility in one region of the cell periphery is constantly compacting and folding the excess membrane-cortex couple which was created by relaxation in a distal portion of the periphery (Fig 1.4).

Fig 1.4 The membrane-cortex exhibits accordion-like folding during contraction. A,B. Example of transmission electron microscopy image of the cell fixed during the oscillation. Yellow rectangle on the (A) shows the position where the magnified image (B) was taken. Extensive folding, sometimes appeared as closed membranes in thin section, is observed on one side of the cell while the distal side is smooth. (C) Schematic view of membrane-cortex folding and unfolding and corresponding confocal images of the membrane (red) and F-actin cortex (green) fluorescent signals during oscillation. The yellow rectangle on the top view (t=0s) shows the position of the rest of images. This figure was provided by Maryna Kapustina.

Fig 1.4

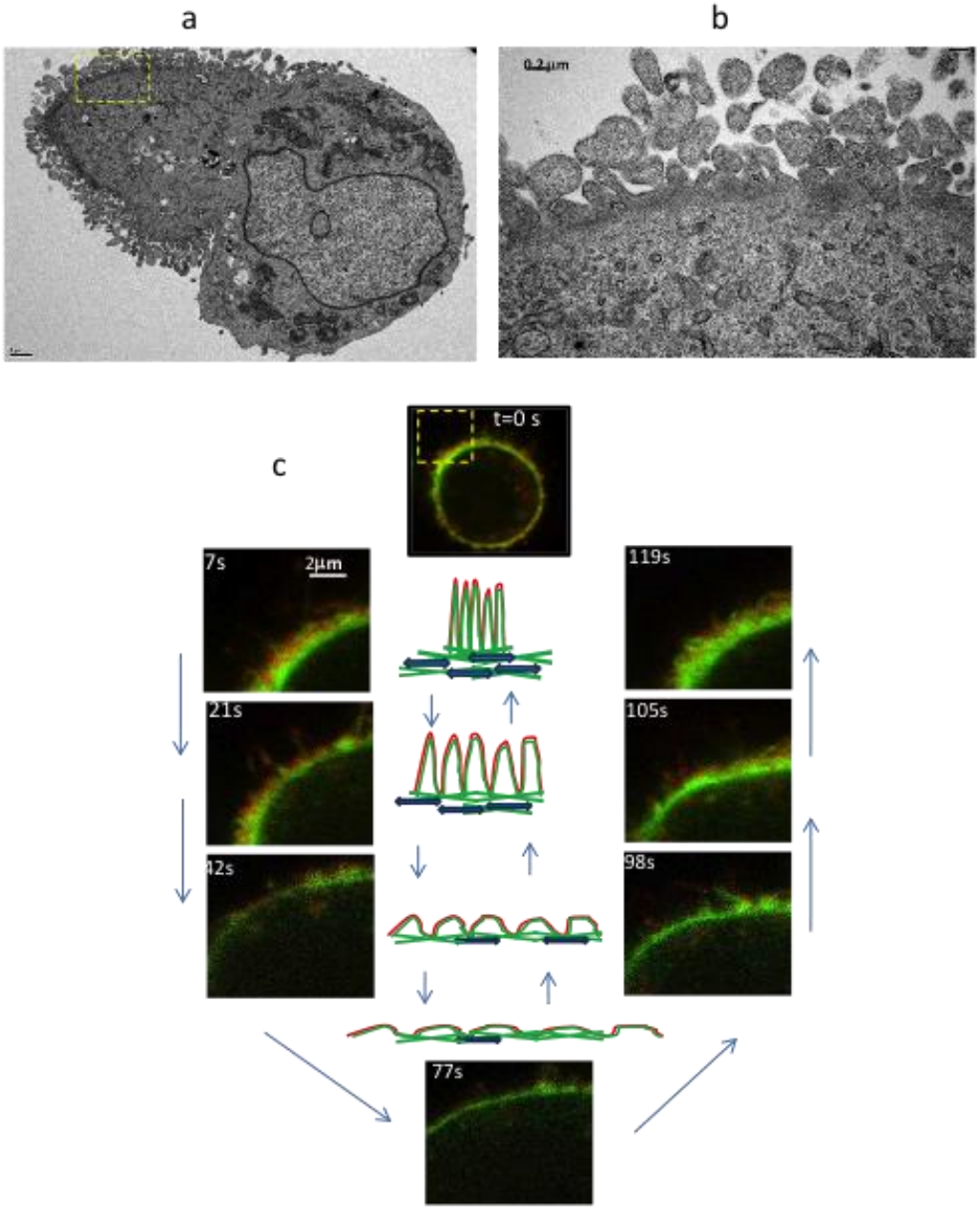

Migration Modes in 3D. Substrate dimensionality and composition greatly affect cell migration morphology and biochemical regulation (Bissell and Barcellos-Hoff, 1987; Cukierman et al., 2002; Dobereiner et al., 2005; Even-Ram and Yamada, 2005; Wolf and Friedl, 2011). In 2D, fibroblasts migrate with flat, well-spread morphologies and are able to do so in the absence of myosin II contractility. In 3D, fibroblasts migrate along matrix fibers, exhibit spindle-like mesenchymal morphologies, and cannot migrate without myosin II contractility (Doyle et al., 2009). This spindle morphology and its associated characteristics are mimicked when cells are plated on 1D fibrils, which is more experimentally malleable than are 3D matrices (Doyle et al., 2009). Spindle morphologies result in uni-axial focal adhesions along the fibril track and appear as one long adhesion unit (Fig. 1.5). In contrast, focal adhesions in 2D migrating fibroblasts appear as puncta at various sites in the adhesion plane.

Fig 1.5 From left to right, confocal images of a fibroblast migrating on a 1D fibril, fixed and stained for α_5 integrin, phosphorylated-FAK at position 397, and FAK. The merged image is shown next. At the right is a 2D spread fibroblast, also with co-immunostaining as a control.(Doyle et al., 2009)

Fig 1.5

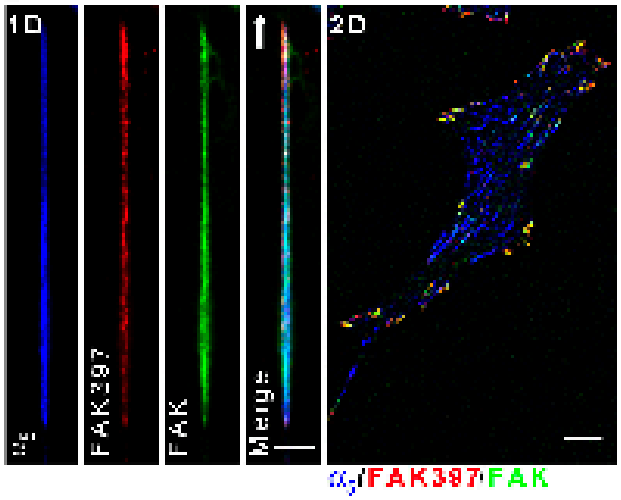

This research was originally published in Journal of Cell Biology. Doyle AD, Wang FW, Matsumoto K, Yamada KM. One-dimensional topography underlies three-dimensional fibrillar cell migration. *Journal Cell Biology*. 2009; 184(4):481-90. © The Rockefeller University Press.

Actin distribution in fibroblasts migrating in 1D and 3D is organized both along the fibril interface and as cortical actin at the circumference of the cell. This is significant as it suggests dynamic cortical actomyosin contractility plays a role in 3D mesenchymal migration. Also, fibroblasts are among the first cells to invade tissues (Wolf and Friedl, 2011), laying down tracks for other cells. This further suggests that structural integrity of the cortex is maintained during protrusions.

Rounded cell amoeboid movement in 3D has lower adhesion to the surrounding environment than does mesenchymal migration, and in general, is not well understood. In many rounded cells, including leukocytes, the rear of the cell contains visibly denser cortex and phosphorylated myosin II, known as a "uropod." The position of the uropod is dependent upon Rho/Rho-kinase and myosin II. Further, the uropod has been shown to co-localize with the substrate binding factors beta-1 integrin, CD44 and PSGL-1, as well as the RhoA-associated factors ezrin, radixin, and moesin (ERM proteins) and PKA, the Golgi complex, and the Microtubule-Organizing Center (MTOC)(Lorentzen et al., 2011; Poincloux et al. 2011). When beta-1 integrin interactions with the substrate are disrupted, the cells undergo periodic protrusions within the 3D matrigel (Poincloux et al. 2011).

Fig 1.6 A375 melanoma cells were plated on a collagen I matrix and imaged with confocal microscopy. Shown is co-staining for phosphorylated myosin light chain and Beta-1 integrin, with apparent concentration of both in the uropod at the rear of cell. Scale bar is 10um.(Lorentzen et al., 2011)

Fig 1.6

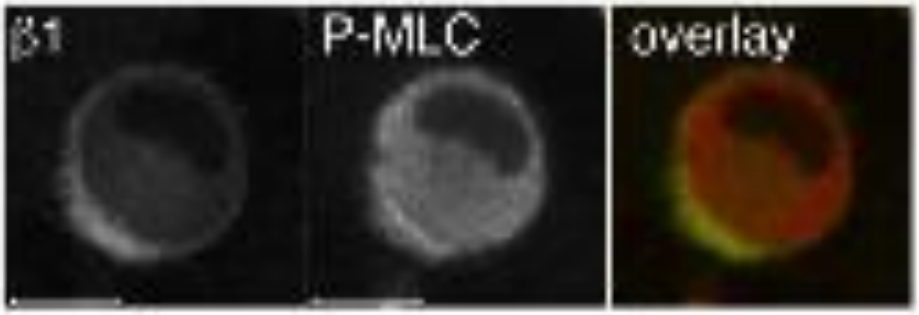

This research was originally published in Journal of Cell Science. Lorentzen A, Bamber J, Sadok A, Elson-Schwab I, Marshall CJ. An ezrin-rich, rigid uropod-like structure directs movement of amoeboid blebbing cells. *Journal of Cell Science*. 2011; 124(8):1256-67. © The Company of Biologists Ltd.

In this work, I show that periodic protrusions, in a manner phenotypically similar to that of uropod studies (Fig 1.6) also exhibit a dense region of cortical actin containing numerous regulatory factors. In periodic protrusions, these density regions travel the circumference of the cell opposite the position of the nucleus during protrusions. Cortical density waves co-localize with RhoA activity, RhoA molecule distribution, myosin II phosphorylation and membrane folding. Further, I use the periodic protrusive phenotype to elucidate the dynamic regulation of the cortex (Chapter 3), which may be applicable to both the uropod cortical density structure as well as other lopobodial-type protrusions.

Migration Mode Regulation. Migration is a dynamic behavior and requires the temporal and spatial regulation of complex signaling networks. Rho GTPases are molecular regulatory switches that allow cells to integrate external and internal cues in a spatiotemporal fashion (Machacek et al., 2009) (Burridge and Wennerberg, 2004). These GTPases may act in concert or as inhibitory factors with one another depending on the migration context. For example, the Rac GTPase is generally responsible for lamellipodia protrusions, such as in leukocytes and in mesenchymal 2D migration (Doyle et al., 2009; Nourshargh et al., 2010; Pankova et al. 2010; Petrie et al., 2009). RhoA GTPase is essential to the myosin II driven protrusions that occur in cortex-driven amoeboid migration. There are numerous examples in which cancer cells transition between these two states by turning on Rac, Rho, or their associated regulatory factors and downstream effectors (Pankova et al. 2010; Sanz-Moreno et al., 2008). Cdc42 GTPase activation has also been shown to induce a mesenchymal

to amoeboid transition and result in increased myosin II activity (Pankova et al. 2010).

Cell movement involves exerting force in order to propel cells forward. During movement, all portions of the cell experience some transduction of force from the cytoskeleton and, to varying degrees, from the substrate. Various signaling molecules are regulated downstream of force transduction in order to achieve the shape changes needed for translocation. Rac1, for example, is inhibited by lateral force on the cell, or stretch (Katsumi et al., 2002), whereas RhoA is activated by force (Bershadsky et al., 1996; Guilluy et al.; Liu et al., 1998; Maddox and Burridge, 2003; Riveline et al., 2001).

Attachment to the extracellular environment and subsequent force transduction in most cells is accomplished via specific combinations of integrin dimers (α and β subunits) embedded in the plasma membrane. Integrin dimers bind matrix ligands such as fibronectin, collagen, laminin, as well as the cell surface receptors ICAM-1 and VCAM-1 (Huttenlocher and Horwitz, 2011). Once bound to the ligand, integrins form clusters and associate with focal adhesion proteins and regulatory factors that form a 40nm deep complex into the cell (Kanchanawong et al., 2010), which transmits extracellular forces to the actin network, see Fig 1.7.

Fig 1.7 Schematic demonstrating the measured spatial relationship between integrins, various focal adhesion proteins and the actin network. The orientation of the force-sensitive protein talin appears to provide scaffolding for the focal adhesion structure. These measurements were found using iPALM, interferometric photoactivatable localization microscopy, which enabled fluorophore-level localization of each protein. (Kanchanawong et al., 2010)

Fig 1.7

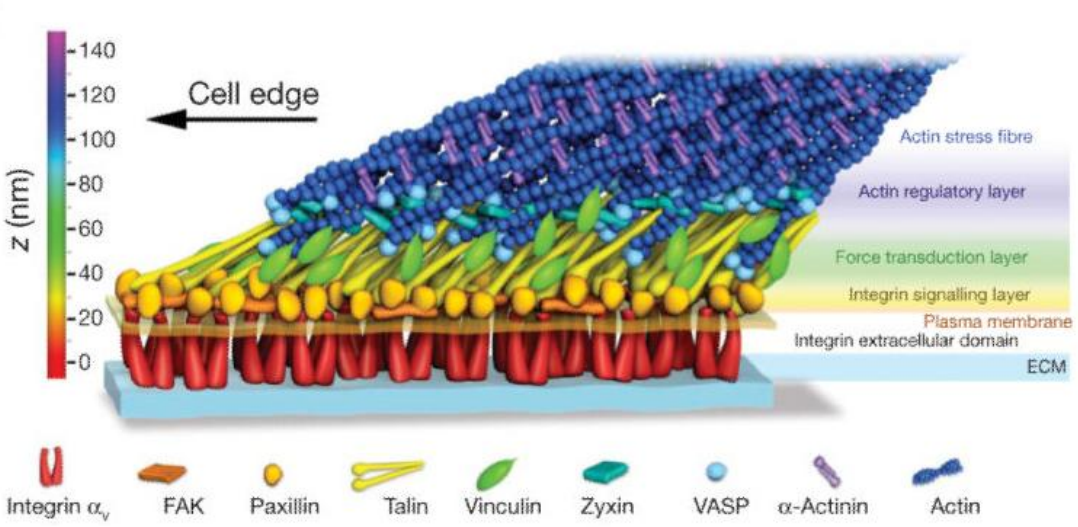

Reprinted by permission from Macmillan Publishers Ltd: [NATURE] Kanchanawong P, Shtengel G, Pasapera AM, Ramko EB, Davidson MW, Hess HF, Waterman CM. Nanoscale Architecture of integrin-based cell adhesions. 468(7323): 580-4, 2010.

Focal adhesions form and dissociate in a force-dependent, RhoA-mediated manner. When the RhoA effector Rho-kinase (ROCK) is inhibited, focal adhesions fail to form and only smaller focal complexes arise at the edge of lamellipodia (Geiger et al., 2001; Nobes and Hall, 1995; Rottner et al., 1999). Downstream of ROCK, myosin II contractility determines not only focal adhesion size (Stricker et al., 2011) but also protein localization (Kuo et al. 2011). Myosin II contractility also regulates the growth and dissociation rates of focal adhesions. Focal adhesion molecule turnover is primarily regulated by the k_{off}, or dissociation rate; myosin II contractility decreases the k_{off} for the FA protein vinculin and increase the k_{off} rates for paxillin and zyxin (Wolfenson et al., 2011). At the same time, a number of FA proteins have been shown to extend their conformation in response to force, thus changing their molecular affinities and subsequent signaling. Coupled with a dynamic actin polymerizing network, focal adhesions appear to act as "molecular clutches" during migration (Gardel et al., 2010; Hoffman et al., 2011) in which the force of polymerizing actin, as well as associated myosin II contractility, is transmitted to the substratum in a controlled manner via FAs, propelling cells forward.

Activation of RhoA via force occurs through the integrin-mediated pathways FAK-Erk-GEFH1 and via the Src-kinase family Fyn activation of the RhoGEF LARG (Guilluy et al. 2011). Interestingly, GEFH1 distribution to focal adhesions was found to be dependent on myosin II activity (Kuo et al. 2011). These data suggest a positive feedback from myosin II to GEFH1 in focal adhesion maturation. In this work, we show that GEFH1 activity is also dependent on myosin II.

Although the mechanisms suggested here for 2D planar migration are likely relevant in rounded cell morphologies, very little is known about dynamic regulation of the cortex and its force transduction during migration. In rounded and 3D migrating cells, adhesion area is decreased and cortical actin is increased. In this work, I show evidence that the actomyosin cortex of rounded cells is capable of force transduction and mechanochemical signaling independently of integrin signaling. Our data indicates that a positive feedback exists between myosin II and GEFH1 in both the spread and rounded states. In the case of a spread cell, this has been shown to occur via (Guilluy et al. 2011) integrin signaling. In the case of a rounded cell, I show that this is integrin indepenent. I propose that this mechanism of dynamic cortical regulation drives protrusions and facilitates rounded cell motility, in a manner that may also involve integrin engagement, as cells navigate dense 3D environments.

CHAPTER 2

EVIDENCE IMPLICATES RHOA, RATHER THAN CALCIUM, AS THE PRIMARY OSCILLATING REGULATOR OF PERIODIC PROTRUSIONS

Introduction

When microtubules are depolymerized in spreading cells, they experience morphological oscillations characterized by a period of about a minute, indicating that normal interactions between the microfilament and microtubule systems have been significantly altered. This experimental system provides a test bed for the development of both fine- and coarse-grained models of complex motile processes, but such models need to be adequately informed by experiment. Using criteria based on Fourier transform analysis, we detect spontaneous oscillations in spreading cells. However, their amplitude and tendency to operate at a single frequency are greatly enhanced by microtubule depolymerization. Knockdown of RhoA and addition of various inhibitors of the downstream effector of RhoA, Rho kinase, block oscillatory behavior. Inhibiting calcium fluxes from endoplasmic reticulum stores and from the extracellular medium does not significantly affect the ability of cells to oscillate, indicating that calcium plays a subordinate regulatory role compared to Rho. We characterized the dynamic structure of the oscillating cell by light, fluorescence, and electron microscopy, showing how oscillating cells are dynamically polarized in

terms of their overall morphology, f-actin and phosphorylated myosin light chain distribution, and nuclear position and shape. Not only will these studies guide future experiments, they will also provide a framework for the development of refined mathematical models of the oscillatory process.

Periodic morphological oscillations in spreading cells were first observed after depolymerization of microtubules (MTs) with colcemid (Pletjushkina et al., 2001). It was shown that actin, myosin, and Rho kinase were needed for oscillations to propagate, and that the oscillation phenotype could be induced in a number of cell types, including fibroblasts, epithelial cells, and lymphoblasts (Paluch et al., 2005; Pletjushkina et al., 2001; Salbreux et al., 2007). Other groups have found that suspended cells undergo morphological oscillations with or without depolymerized MTs, and that when MTs are depolymerized, periodic local ruptures of the actomyosin cortex occur that initiate the oscillations (Paluch et al., 2005) . In general, this periodic cell volume displacement provides a window into interactions between the actomyosin and MT systems that occur in rounded cells. One of the consequences of MT depolymerization is an increase in the concentration of RhoGEF-H1, which raises the level of active RhoA (Krendel et al., 2002).

In a previous work, we putforward a working hypothesis that an increment in Rho activity puts the cell in a more contractile state; this state is modulated by periodic influxes of calcium that produce a periodic increase in calmodulin-mediated activation of myosin light chain kinase (Pletjushkina et al., 2001). To complete the mechanism, it was postulated, a negative feedback occurs between increasing

contractility and the calcium influx (Weinreb et al., 2006). The elements of our hypothesis were investigated by employing both a new coarse-grained systems cell biology approach termed causal mapping (CMAP) (Weinreb et al., 2006)and a traditional ordinary differential equation formulation (Kapustina et al., 2008) to show that this scheme could, in fact, produce oscillations. A cortical actin gel mechanochemical model of oscillations using similar calcium-based regulatory mechanisms has also been put forward (Salbreux et al., 2007). The oscillatory phenomenon presents an example of the analysis of a complex mechanochemical system at the cellular level that serves as a challenge for both systems cell biology approaches and more conventional modeling efforts. We used an advanced CMAP technology termed hypothesis generation to investigate which of many different pathway architectures are capable of producing cortical oscillations (Weinreb et al., 2009). The CMAP modeling effort revealed two competing pathways that create the oscillatory phenotype; one in which calcium plays a leading role, the other in which RhoA is predominantly involved. We sought to further investigate the structural and biochemical factors underlying the oscillation phenomenon, thereby informing the modeling process.

We demonstrate that spontaneous oscillations exist in spreading cells and that the oscillation amplitude and the percentage of cells that oscillate are greatly enhanced by MT depolymerization. Our investigations using fluorescence and electron microscopy revealed that oscillating cells are dynamically polarized in terms of their overall morphology and the distributions of f-actin and active myosin. In

addition, we observed dramatic changes in both the position and shape f the nucleus during the oscillation cycle. We were surprised to find that these periodic contractions of the cortex are not regulated by calcium flux: fully suppressing calcium fluxes from endoplasmic reticulum stores and from the extracellular medium did not inhibit oscillations. Knockdown of RhoA and inhibition of the downstream effector of Rho, Rho kinase, did inhibit oscillations, indicating that RhoA plays a dominant role in the regulation of periodic contractions in this context. Also, direct activation of RhoA through alternate pathways was not sufficient to induce oscillations. Our experimental results necessitate a revision of previous mathematical models of this phenomenon in which the regulation of intracellular calcium underlies the oscillatory behavior; to this end, we propose a mechanism for oscillations in which the dominant factor is the spatiotemporal regulation of RhoA.

Materials and Methods

Phase contrast imaging. Cells were transferred to a Nikon Diaphot 300 microscope (Melville, NY.) with a 37 C open perfusion microincubator (model PDMI-2, Harvard Apparatus Inc., Holliston, MA.) and a 5% CO2 solution was perfused into the chamber. Phase contrast images were taken at 10 s intervals at 20x magnification for a period of 0.5-2 h after cell plating using a Hamamatsu (Bridgewater, NJ.) dual mode cooled CCD camera C4880 and recorded using Metamorph 8.0 software (Molecular Devices, Downington PA.).

DIC and orange calcein-am fluorescence imaging. After the 25 min incubation time, cells were transferred to an Olympus (Center Valley, P.A.) IX-81 microscope. The temperature was maintained at 37 C by a Warner Instruments (Hamden, C.T.) incubator and a 5% CO2 solution was perfused into the chamber. Images were obtained with a SensiCam QE CCD camera (Cooke Corporation, Romulus, M.I.) at 10s intervals and recorded and processed with Metamorph 8.0 software. DIC images were taken at 60x magnification. Orange calcein-am fluorescence imaging was interspersed sequentially with phase contrast at 20x magnification.

Quantification of cell oscillations. The area of analysis was defined for each cell individually, as cells varied in size and shape. The area of analysis included only single cells not in contact with other cells (see Fig. 2.1 A and Fig. 2.2). All cells in the population meeting this criterion were included in the population analysis. We

developed a Matlab (Mathworks, Natick, MA.) program to automate the analysis of isolated cells. For each frame, the center of intensity (X_{CI}, Y_{CI}) was calculated as follows:

$$\left(X_{CI}, Y_{CI}\right) = \sum_{j=1}^{r} \sum_{i=1}^{c} I_{ij}\left(x_{ij}, y_{ij}\right) / \sum_{j=1}^{r} \sum_{i=1}^{c} I_{ij} \qquad \text{(S1)}$$

where the sums are over the r rows and c columns of the selected area and I_{ij} and (x_{ij},y_{ij}) are the intensity and position of the (i, j)th pixel, respectively. A time series for the center of intensity consisting of 256 frames (corresponding to 50 min) was used to compute the power spectrum of the Fourier transform for all experiments except those in which the media was changed or a reagent was added after the onset of oscillations; in such cases, 128 frames corresponding to 25 min were used for each experiment. This observation window was chosen as the ideal time frame based on the fact that the cells maintained a fairly consistent morphology during this time, were well attached, and did not move out of the frame. We excluded period values above 400 s from the power spectrum, as these correspond to irrelevant longer time scale trends in the signal. We then normalized the remainder of the signal values so that the discrete values added to 1. Power spectra from both the x and y axes (Fig. 2.1 A) were compared for each cell, and the axis exhibiting the largest spectral amplitude meeting our criteria was selected to characterize the oscillation period for that cell. Only cells that oscillated with periods within the range of 40-120 s were considered in the analysis. Cells with periods below 40 s were excluded because our frequency of

Fig 2.1 In our analysis, each oscillating cell is analyzed for displacement of the center of phase contrast intensity as a function of time. (A) Phase contrast (20x) image of a spreading Swiss 3T3 cell treated with colchicine (bar =20 um). The area of analysis is designated by hand. The x and y axes are analyzed individually to find the center of intensity as described in Materials and Methods. (B) The temporal variation of the position of the first moment of intensity along a single axis from both calcein-orange (red) and phase contrast (black) images of an oscillating cell are shown. In contrast to the phase contrast signal, (the fluorescent signal is subject to probe bleaching. Both the phase contrast and the fluorescence signal are in phase and give similar periods but the amplitude of the fluorescent signal is smaller by a factor of 10 as compared to the phase contrast signal. Fig. 2.1 C-E give examples of Fast Fourier Transform power spectra calculated from the excursions of the first moment of intensity along a single axis for three different cells imaged with phase contrast. Several criteria were employed so that only cells with highly periodic signals were used for analysis. In each figure, the two horizontal dotted lines are the mean amplitude and the "mean + the 3 std dev" amplitude value. The vertical dotted lines show the 10 s interval surrounding the maximum amplitude value. In Fig. 2.1 C, the cell has no predominant power spectrum peak and is therefore considered non-oscillating. In Fig. 2.1 D, the cell has frequency peaks above the threshold of "mean + 3 std dev" that we established, however, these frequencies are more than 10 s apart and the satellite peaks are more than ½ the dominant peak. Therefore we do not include this cell as

oscillating. In Fig. 2.1 E, the cell has a dominant peak that meets the aforementioned criteria, and we therefore consider this cell as “oscillating.”

Fig 2.1

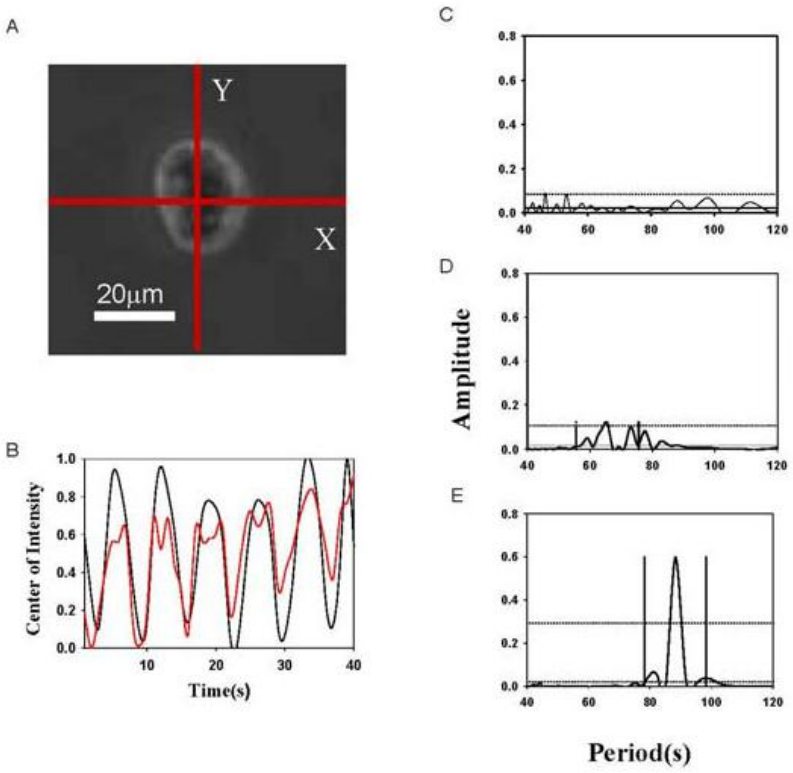

image acquisition (10 s between frames) was not sufficient to properly sample those oscillations. Cells with periods above 120 s were excluded as outliers because their periods were greater than three standard deviations above the mean period.

To simplify our study of the oscillation period, we limited our analysis to cells with a single frequency. A cell is considered to be oscillating with a single frequency if the following criteria are met: i) the largest peak amplitude value must be greater than three standard deviations above the average amplitude of the spectrum (as seen in Fig. 2.1 D and E); ii) when more than one peak is above threshold and the associated periods differ by more than 10s, the maximum peak must have a spectral amplitude at least twice as large as that of the secondary peak (as seen in Fig. 2.1 E). If the difference between two peaks is less than 10s, we use the largest peak as representative of the cell's period. Fig. 2.1 C and D represent non-oscillating cells based on these criteria, whereas Fig. 2.1 E represents an oscillating cell. Power spectra from both the x and y axes (Fig. 2.1 A) were compared for each cell, and the spectrum from the axis exhibiting the largest amplitude meeting our criteria was selected to characterize the oscillation period for that cell.

The amplitude of the signal was determined from averaging the difference between each consecutive maximum and minimum (extrema) of the center of intensity signal along a given axis. The amplitude is thus defined as:

$$\frac{\sum_{i=1}^{N}\left|x_{i+1}-x_i\right|}{N-1} \qquad \text{(S2)}$$

where N=number of extrema, i=index of extrema, and x_{i+1}- x_i is the particular amplitude. We also categorize all cells that have average amplitudes less than that which was observed by the same analysis of the background light transmission of a phase contrast image (equivalent to 0.05 μm) as non-oscillating.

We confirmed that the use of phase contrast was a valid measurement for changes in the distribution of cell volume during the oscillatory cycle by co-imaging the fluorescent volume indicator, calcein-AM, with phase contrast. The center of mass for both signals was calculated as described above. To compare signals, we normalized the amplitudes of both signals to show that the first moment of the volume signal and phase contrast intensity of the oscillating cell are essentially in phase and have the same period (Fig. 2.2).

Fig 2.2 20x phase contrast image of spreading confluent Swiss 3T3 cells treated with colcemid. The white boxes are selected by hand in Matlab for analysis of the center of intensity within the area over time. Only cells not in contact with other cells were chosen for the analysis.

Fig 2.2

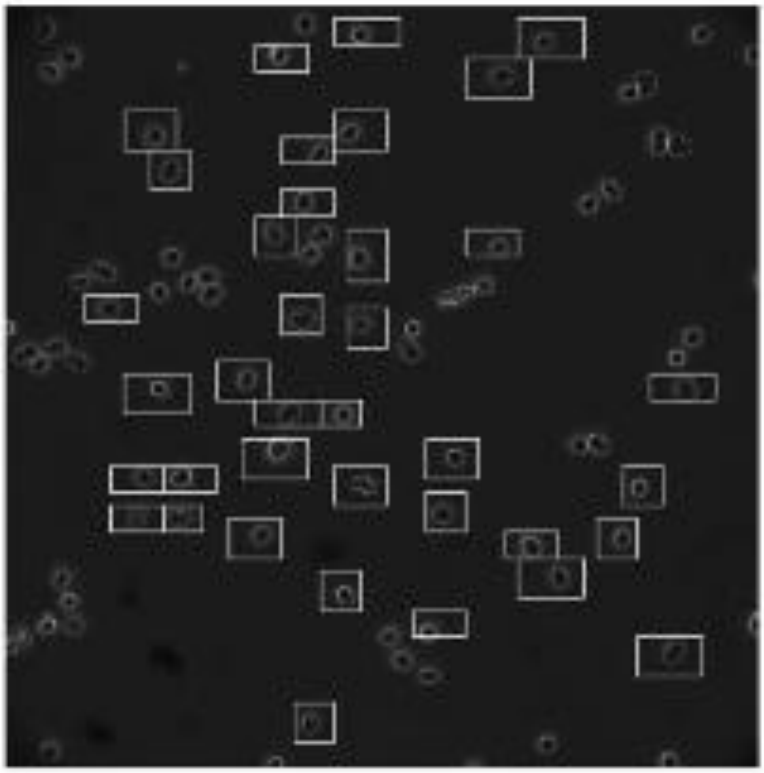

Immunofluorescence and f-actin and nuclear staining. After fixation with 3.7% formaldehyde for 15 min at 37°C, cells were permeabilized with 0.1% Triton-X100 for 20 min. Cells were then washed with PBS and stained with AlexaFluor-594-phalloidin (Molecular Probe) for 20 min or with 500 nM DAPI (4',6-diamidino-2-phenylindole, Molecular Probe) in PBS at room temperature for 5 min.

Rabbit phospho-myosin light chain 2 (Ser19) antibody (anti-pMLC; Cell Signaling) was used for indirect immunostaining of phosphorylated myosin light chain. For indirect immunostaining, cells were plated on glass bottom dishes (Mattek-35mm) with a 10 μg/ml fibrinogen precoating. 10 μM colchicine was added during the plating. Cells were imaged using phase contrast microscopy every 10 s to ensure that they exhibited morphological oscillations. After 30 min of defined oscillations, cells were fixed with 4% formaldehyde for 15 min, washed and incubated for 1 h in blocking buffer (PBS+5% goat serum+0.4% Triton), then washed with PBS and incubated overnight in 4ºC with rabbit anti-pMLC. Cells were then incubated for 2 h at room temperature with fluorescently labeled secondary antibodies (Alexa Fluor488 goat anti-rabbit, 1:2000, Invitrogen). Images were acquired using an Olympus FluoView1000 confocal scanning microscope Olympus FluoView1000 with a 60x water immersion objective

Results

Microtubule depolymerization enhances oscillations that occur spontaneously in spreading cells

spontaneously in spreading cells. Fig. 2.3 A shows a representative kymograph of a Swiss 3T3 cell after the addition of 10 μM colchicine. The period of this cell oscillation is about 60 s and is visible in the excursions of the cell periphery of ~ 1.5 μm. The inset in Fig 2.3 shows the region of the cell from which the kymograph is taken. The increase in amplitude of the oscillatory signal after a single CHO cell is treated with 10 μM colchicine is shown in Fig. 2.3 B which gives the waveform before (solid line) and after microtubules are depolymerized (dotted line). The power spectra of the waveforms in Fig. 2.3 C show the concentration of power in a narrow frequency range after treatment with colchicine. About 50% of CHO and Swiss 3T3 spreading cells spontaneously oscillated and met our criteria (see Methods) for single frequency oscillations during the observation window of 1-2 h after plating (Fig. 2.4 A). The amplitude of the oscillation signal (see Methods) was consistent over multiple cell passages and responded consistently to reagent treatment. We found that the average amplitude of untreated oscillating CHO cells was 0.15 ± 0.04 μm [N=360] and of untreated oscillating Swiss 3T3 was 0.18 ± 0.02 μm [N=277] (Fig. 2.4 B). Cells with depolymerized microtubules oscillated with an average amplitude that was slightly more than twice the amplitude of untreated cells, 0.33 ± 0.03μm for CHO cells [N=221] and 0.38 ± 0.03 μm for Swiss 3T3 [N=135]. Microtubule depolymerization also significantly increased the percentage of oscillating CHO cells to an average of 80% [N=221] and of oscillating Swiss 3T3 to 85% [N=135] (Fig. 2.4

A and B). The average period value varied within the range of 83 ± 12 s [N=2,588] and did not exhibit consistent response patterns to reagent treatment.

Fig 2.3 Dynamics of the oscillatory phenotype. (A) Kymograph of a peripheral section (see inset) of a Swiss 3T3 cell undergoing oscillations induced by colchicine and imaged at 60x in DIC. The section used for the kymograph is 2x20 pixels wide and is obtained from 46 images taken every 10s. (B) The center of phase contrast intensity (see Methods) as a function of time for a single CHO cell before (black) and after 15 minutes of treatment with colchicine (red). Note the increase in amplitude that occurs after depolymerization of microtubules. (C) Corresponding power spectra from the Fourier Transform of the waveforms in B shows concentration of power in a narrow range of frequencies after colchicine treatment.

Fig 2.3

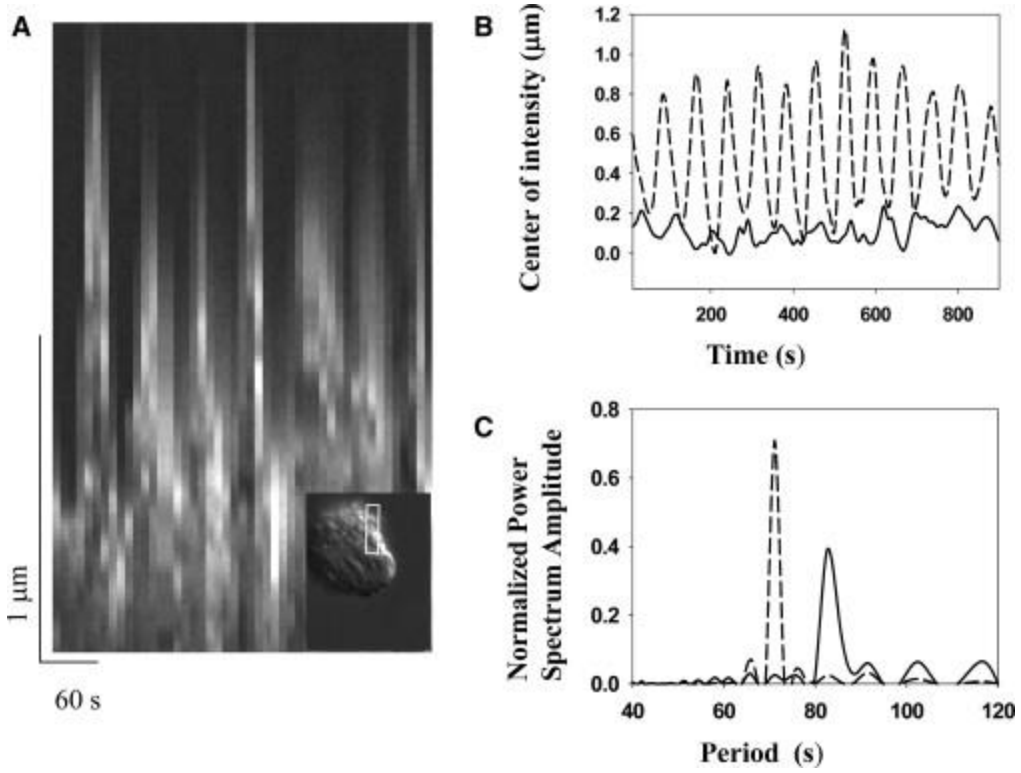
A
1 µm
60 s
B
Center of intensity (µm)
1.2
1.0
0.8
0.6
0.4
0.2
0.0
200
400
600
800
Time (s)
C
Normalized Power Spectrum Amplitude
0.8
0.6
0.4
0.2
0.0
40
60
80
100
120
Period (s)

Fig 2.4 Microtubule depolymerization enhances oscillations that occur spontaneously in spreading cells. (A) The average percentage of oscillating cells per experiment was measured as described in Methods. Treatment with colchine (10μM) or colcemid (1 μM) increases the percentage of oscillating cells. (B) The average amplitude of oscillating cells per experiment was analyzed as described in Methods and doubles with microtubule depolymerization.

Fig 2.4

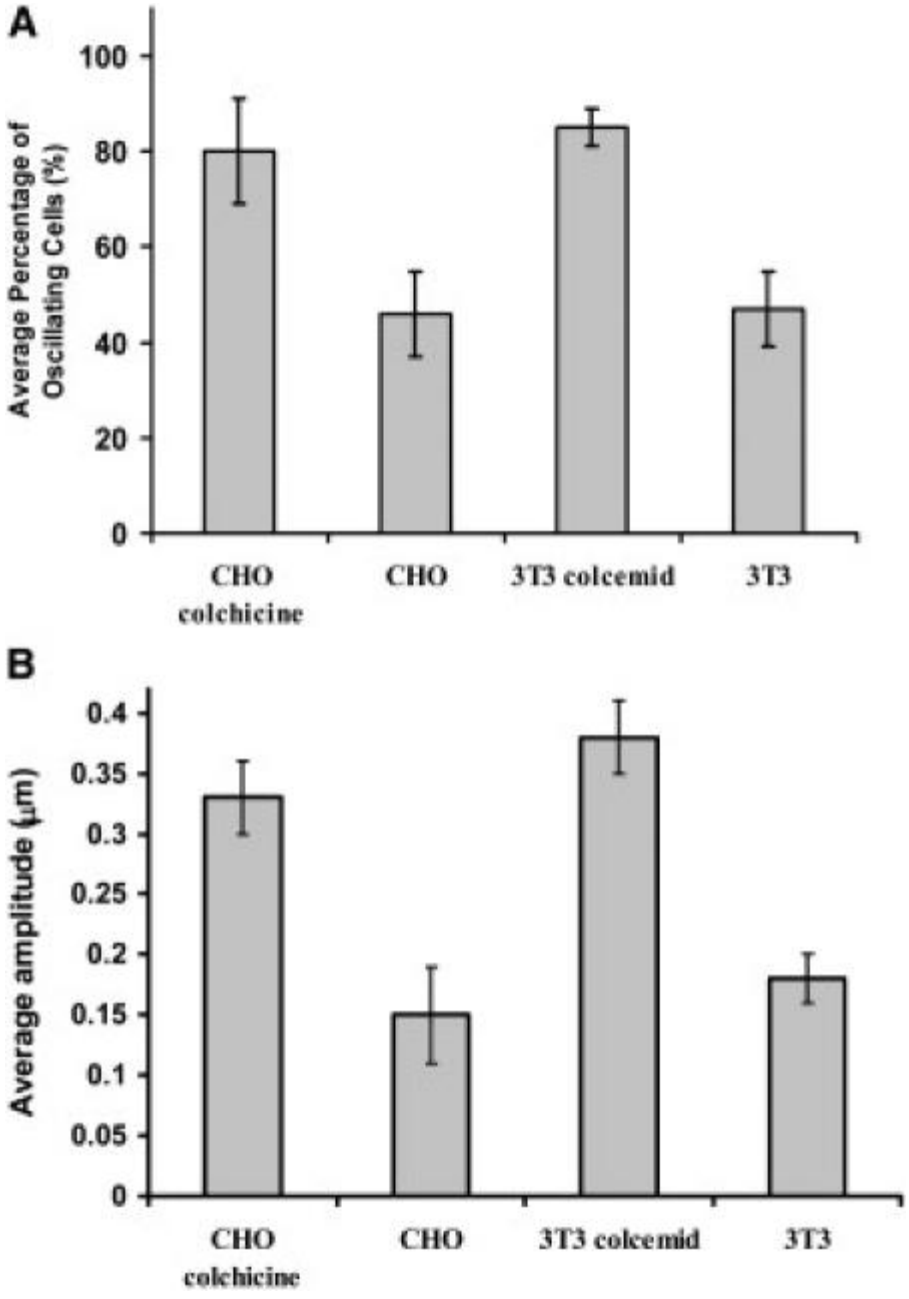
A
Average Percentage of Oscillating Cells (%)
100
80
60
40
20
0
CHO colchicine
CHO
3T3 colcemid
3T3
B
Average amplitude (μm)
0.4
0.35
0.3
0.25
0.2
0.15
0.1
0.05
0
CHO colchicine
CHO
3T3 colcemid
3T3

Cell morphology during oscillations. We imaged cells that had been fixed during oscillations using scanning electron microscopy. A representative image (Fig. 2.5 A) shows a convoluted surface that indicates a reservoir of folded membrane, an expected property for rounded cells. The image also suggests considerable height in the oscillating cells. To visualize the shape of the cell cortex, oscillating cells were fixed and stained with rhodamine phalloidin for f-actin. Laser scanning confocal microscope images were acquired at multiple image planes along the z axis to permit three-dimensional actin isosurface reconstructions using Image Surfer software. Fig. 2.5 B-D show several typical examples of cell morphology detected by 3D reconstruction. Fig. 2.5 C and D present top (C) and side (D) views of the same cell which exhibits morphological similarities to the SEM image. Many cells have bulges or extensions on one side. The height of the cell during oscillations, sometimes reaching over 20 μm, is remarkable.

Calcium plays a subordinate role in oscillations. We tested our previous hypothesis that $[Ca^{2+}]_i$ flux was driving cell oscillations, either via stretch activated calcium channel entry from the extracellular media or through endoplasmic reticulum (ER) mediated calcium uptake. We found through the use of various inhibitors and by intracellular free calcium imaging that calcium flux is not required for the propagation of cortical oscillations. Depriving cells of extracellular calcium ([N=74], Fig. 2.6 A and B), or adding the ER ATPase inhibitor thapsigargin ([N=306], data not shown) did not halt oscillations, indicating that neither extracellular nor intracellular sources of calcium flux were involved in regulating oscillations. The percentage of

Swiss 3T3 cells that continue to oscillate in the presence of the endoplasmic reticulum (ER) SERCA pump blocker, thapsigargin, did not change appreciably, either with [N=100] or without microtubule depolymerization [N=206]. To examine the effects of media containing no extracellular calcium on cell oscillations, cells were plated in serum-free media containing calcium and were observed in phase contrast. The media was then removed and cells were washed and then incubated with serum-free media containing no calcium. We observed that Swiss 3T3 cells with and without colchicine continue oscillating in the absence of extracellular calcium. However, cells treated with colchicine (which causes microtubule depolymerization) in serum-free medium did not remain sufficiently attached during the change of media to quantify oscillations with our technique; therefore, we added 5 mM of the calcium chelator EGTA to colchicine treated cells plated in serum-containing media (Fig. 2.6 C and D). We found that all of these cells ([N=37]) continue oscillating after extracellular calcium chelation (media contains 2 mM calcium).

We also performed intracellular calcium ratiometric imaging using Fura-2. We detected no discernible and reproducible spatiotemporal gradients that correlated with the pronounced morphological oscillations (data not shown), consistent with the thesis that changes in $[Ca^{2+}]_i$ due to fluxes from the extracellular media and from ER stores do not play a dominant role in regulating cortical oscillations in spreading cells.

Fig 2.5 Views of the morphology of oscillating cells. (A) Scanning electron microscope image of an oscillating cell. (B-D) 3D reconstruction and visualization of f-actin isosurface for low threshold values of fluorescence intensity (i=250 a.u.) using ImageSurfer software. Cells were induced to oscillate, fixed and stained with rhodamine phalloidin for f-actin. Twelve sections with 1 μm steps along the z axis were imaged using a laser scanning confocal microscope. Maryna Kapustina provided Fig 2.5 B-D.

Fig 2.5

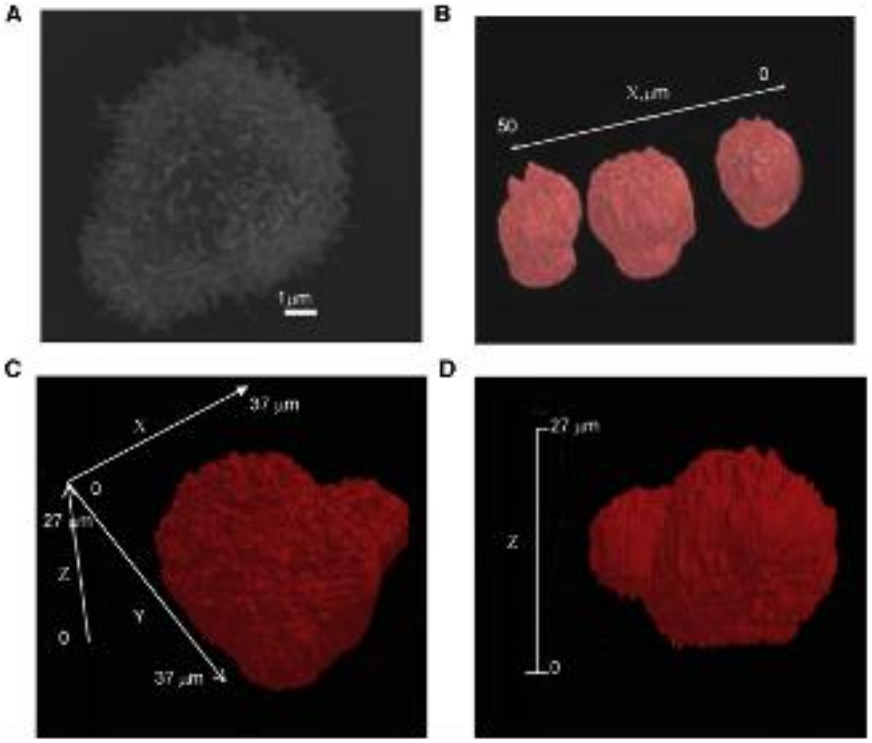

Fig 2.6 Removal of extracellular calcium or addition of the calcium chelator EGTA does not affect the ability of a cell to oscillate. (A,C) Phase contrast derived center of intensity signals of a spontaneously oscillating Swiss 3T3 cell before and after removal of calcium (A) as described in text, and of a cell induced to oscillate by colchicine before and after addition of EGTA (C). (B,D) Power spectra of the cells before (black) and after (red) removal of calcium and of addition of EGTA corresponding to A and C, respectively. Maryna Kapustina provided the cells shown in Fig 2.6C-D.

Fig 2.6

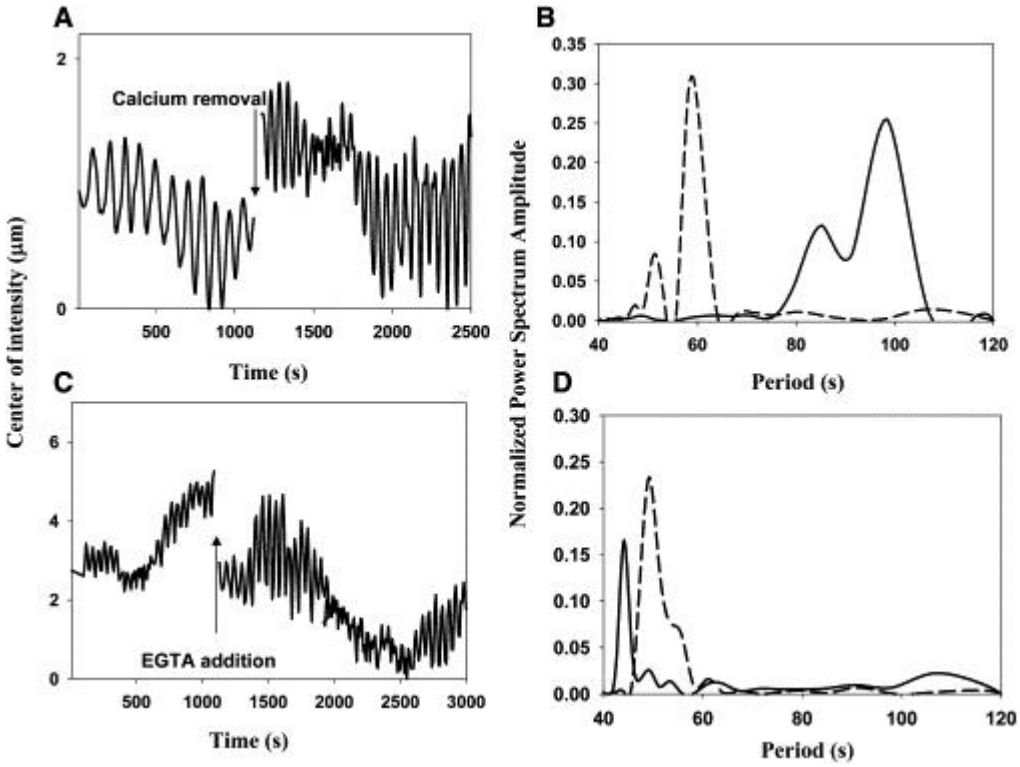
A
Calcium removal
Center of intensity (µm)
Time (s)
B
Normalized Power Spectrum Amplitude
Period (s)
C
EGTA addition
Time (s)
D
Period (s)

RhoA/ROCK pathway is essential. Microtubule depolymerization, known to activate RhoA by releasing RhoGEF-H1 (Krendel et al., 2002) increases the amplitude of oscillations and the percentage of oscillating cells (Figs. 2.3 and 2.4). Thus we asked whether microtubule depolymerization induces oscillations primarily through activation of RhoA. Inhibiting RhoA with the siRNA to human RhoA significantly decreases the percentage of cells induced to oscillate with colchicine vs. the siRNA control. The percentage of cells oscillating with the scrambled human siRNA control was similar to the percentage of cells oscillating with electroporation alone (65% [N=51]), demonstrating that the effect of RhoA siRNA on oscillations is RhoA specific. Further, inhibition of the downstream effector of Rho, Rho kinase (ROCK), by three different inhibitors in cells treated with colchicine immediately halts oscillations. It was previously shown (Paluch et al., 2005; Pletjushkina et al., 2001) that both HA-1077 and Y-27632 caused immediate cessation of colcemid-induced oscillating cells. Using the analysis described in Methods, we quantified the previously published Y-27632 results, and also employed the more specific ROCK inhibitor H-1152 (Ikenoya et al., 2002); both of these inhibitors caused immediate cessation of oscillations.

Global activation of RhoA though pathways other than microtubule depolymerization (LPA at commonly used concentrations (1 μg/mL [N=47], 4 μg/mL [N=41], and 8 μg/mL [N=192]), or treatment with 1 U/mL thrombin [N=90],) do not cause significant increases in the amplitude or the percentage of Swiss 3T3 and CHO cells that oscillate. These data demonstrate that the RhoA pathway is needed

for the regulation of cortical oscillations, but that in contrast to microtubule depolymerization, global activation of alternate RhoA activating pathways does not enhance the ability of a cell to oscillate.

Downstream of RhoA, MLC phosphatase is inhibited by ROCK but can also be inhibited by the addition of the calyculin reagent, thereby increasing global MLC phosphorylation. A moderate concentration of calyculin (25 nM) decreases the percentage of oscillating Swiss 3T3 cells by an average of 51% [N=69] (the amplitude remained unchanged), indicating that a global increase in contractility reduces the fraction of cells competent to oscillate. These results suggest that it is the spatiotemporal regulation of RhoA activity and its downstream effectors, as opposed to simply globally elevating these levels, that produces cell oscillations.

Cortex structure during oscillations: Active RhoA increases both MLC phosphorylation and actin polymerization (Aggeler et al., 1991; Arthur and Burridge, 2001; Burridge and Wennerberg, 2004; Machacek et al., 2009; Tsuji et al., 2002). To better understand the regulation of oscillations, which are ultimately powered by actomyosin dynamics, we investigated the spatiotemporal dynamics of actin and myosin during oscillations. Consistent with previous observations (Paluch et al., 2005; Pletjushkina et al., 2001), we found that latrunculin, which blocks actin polymerization, and blebbistatin, which inhibits myosin contractility, both abrogate the oscillatory phenotype in colcemid treated cells. Below we describe our studies of cortical polarization during oscillations.

F-actin is highly polarized during cell oscillations: Having established some features of the oscillating cell's cytoplasmic volume redistribution, it becomes important to ask how this redistribution is related to the contractile actomyosin cortex that presumably drives oscillations. We examined the actin cortex in a population of cells that underwent morphological oscillations induced by colchicine. Fig. 2.7 A presents the phase contract image of 155 cells out of which 145 (93.5%) were oscillating. The oscillating cells were fixed on the stage with 4% formaldehyde and stained with AlexaFluor-594-phalloidin to visualize actin filaments. Fig. 2.7 B and C show that many of the cells have a highly asymmetrical distribution of actin filaments. Because cells were fixed in different phases of the oscillatory cycle, the correlation between the orientation of oscillatory movement and the polarization of actin within a cell could not be investigated. The same cells were later transferred to the Olympus FV1000 laser scanning confocal microscope where a series of images were taken along the z axis at 1 μm steps for several different cells. These series allowed us to reconstruct the f-actin distribution in three dimensions using ImageSurfer software (Fig. 2.7 D-F).

We assume that the value of AlexaFluor-594-phalloidin fluorescence intensity is a reliable indicator of the concentration of f-actin. The reconstruction with a lower threshold value of fluorescence intensity (Fig. 2.7 D) visualizes the entire actin cortex and shows an asymmetrical shape with an extension on the one side of the cell. The overall height of the cell is around 18 μm. 3D visualization employing a higher fluorescence intensity threshold (Fig. 2.7 E and F) demonstrates that the actin

filament concentration is unevenly distributed around the cell cortex: areas of low filament concentration appear as missing parts of the cortex. To quantify this cortical asymmetry, we used line profiles of unthresholded images at different z planes of a fixed cell (Fig. 2.7 H).

Fig 2.7 F-actin polarization in oscillating cells. (A) Phase contrast image (20x) of cells undergoing morphological oscillations induced by colchicine. (B) Cells were fixed on the stage and stained with AlexaFluor-594-phalloidin to visualize actin filaments. The image shows that many of the oscillating cells have a highly asymmetrical distribution of actin filaments. (C) A magnified image of the outlined area in B (dotted line). (D–F) 3D reconstruction of the f-actin distribution for one representative cell. Fluorescence images were taken on an Olympus FluoView1000 laser scanning confocal microscope using a 60x objective. Images along the z axis were taken at 1-mm steps (20 images total) and a 3D reconstruction was accomplished using ImageSurfer software. (D) Side view, isosurface reconstruction, of a low fluorescence intensity theshold (i= 250 a.u.). (E and F) 3D isosurface visualization of a high fluorescence intensity threshold (i = 1000 a.u.), with side (E) and top (F) views of the same cell, in which the actin filament concentration is highly uneven around the cell cortex. (G) Line profiles of the fluorescence intensity along the indicated line drawn on unthresholded images of different z planes of a cell at one time point in the oscillatory cycle. Maryna Kapustina provided this figure.

Fig 2.7

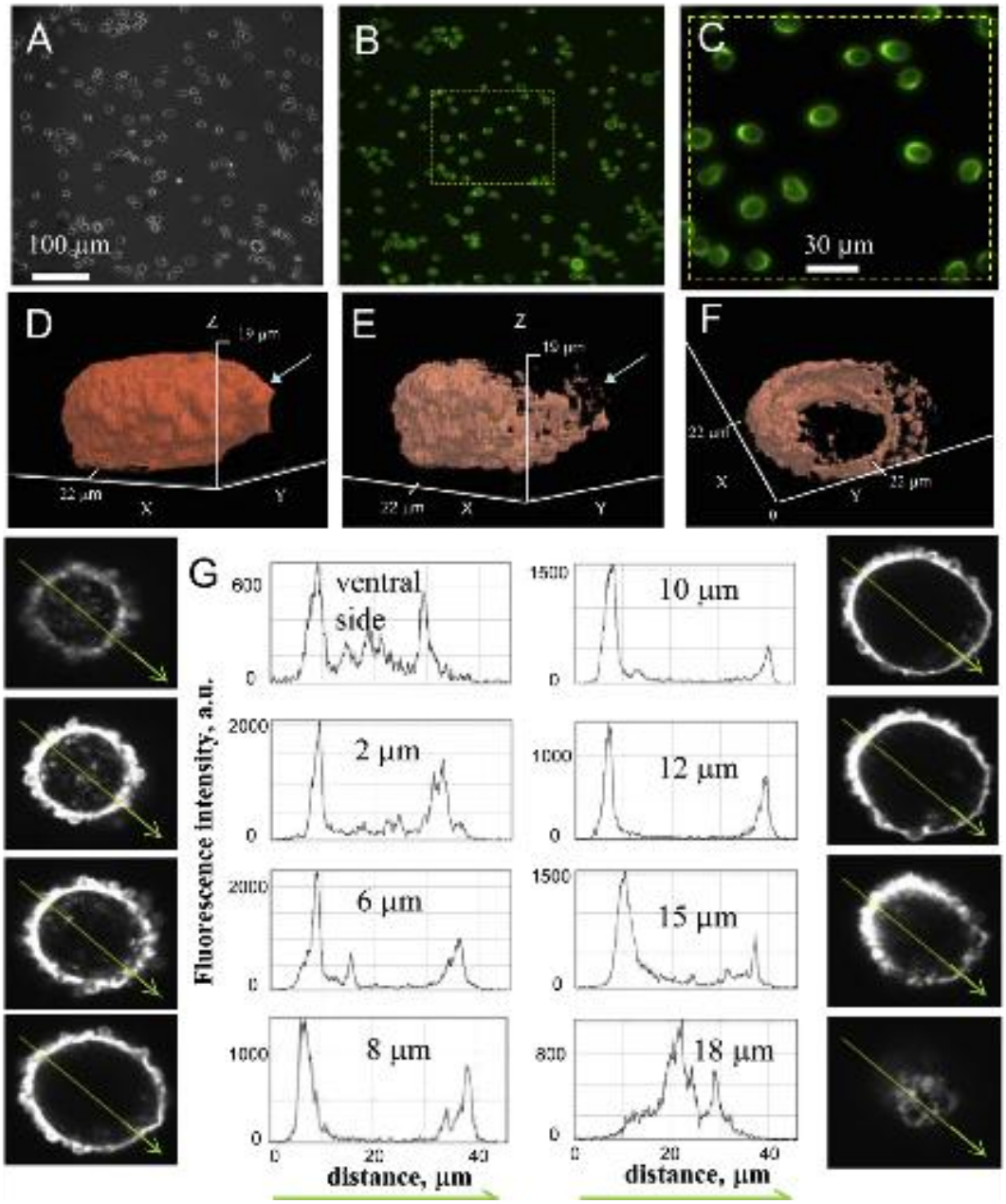
A
100 µm
B
C
30 µm
D
E
F
G
ventral side
10 µm
2 µm
12 µm
6 µm
15 µm
8 µm
18 µm
Fluorescence intensity, a.u.
distance, µm
distance, µm

In our observation of fixed cells, the nucleus is often polarized at one end of the cell, as seen in Fig. 2.8 A confocal section of this cell shows an asymmetric distribution of actin (Fig. 2.8 A) and of active myosin II (Fig. 2.8 B). The co-localization of f-actin and active myosin II in the outer ring is quantified in Fig. 2.8 D and E. The extremely deformed nucleus in the same cell, stained with DAPI (Fig. 2.8 C), is found at one side of the cell, suggesting that it was driven there by intense cortical contractile activity at opposite side of the cell. A 3D reconstruction employing a high fluorescence intensity threshold for actin, phosphorylated myosin light chain, and the nucleus, shows that the nucleus is seemingly pushed towards one side of the cell while the heaviest f-actin and active myosin concentration is concentrated at the other side of the cell (Fig. 2.8 F and G).

Fig 2.8 Concentrations of actin filaments and active myosin are highly correlated. (A–C) Fluorescence images of actin (A) (bar=10 um), phosphorylated MLC (B), and the nucleus (C). In this reconstruction, a high fluorescence intensity (isovalue i =2500 a.u.) was used. Shown are top-view images of the middle of an oscillating cell, which demonstrate the asymmetrical distribution of actin and phosphorylated MLC along with the severely deformed and displaced nucleus. (E) Plot of normalized fluorescence intensity of actin filaments (red) and phosphorylated MLC (green) along the cell perimeter (D) as a function of point number. (F–G) 3D reconstructions of actin (red), phosphorylated MLC (green), and the nucleus (blue). Maryna Kapustina provided this figure.

Fig 2.8

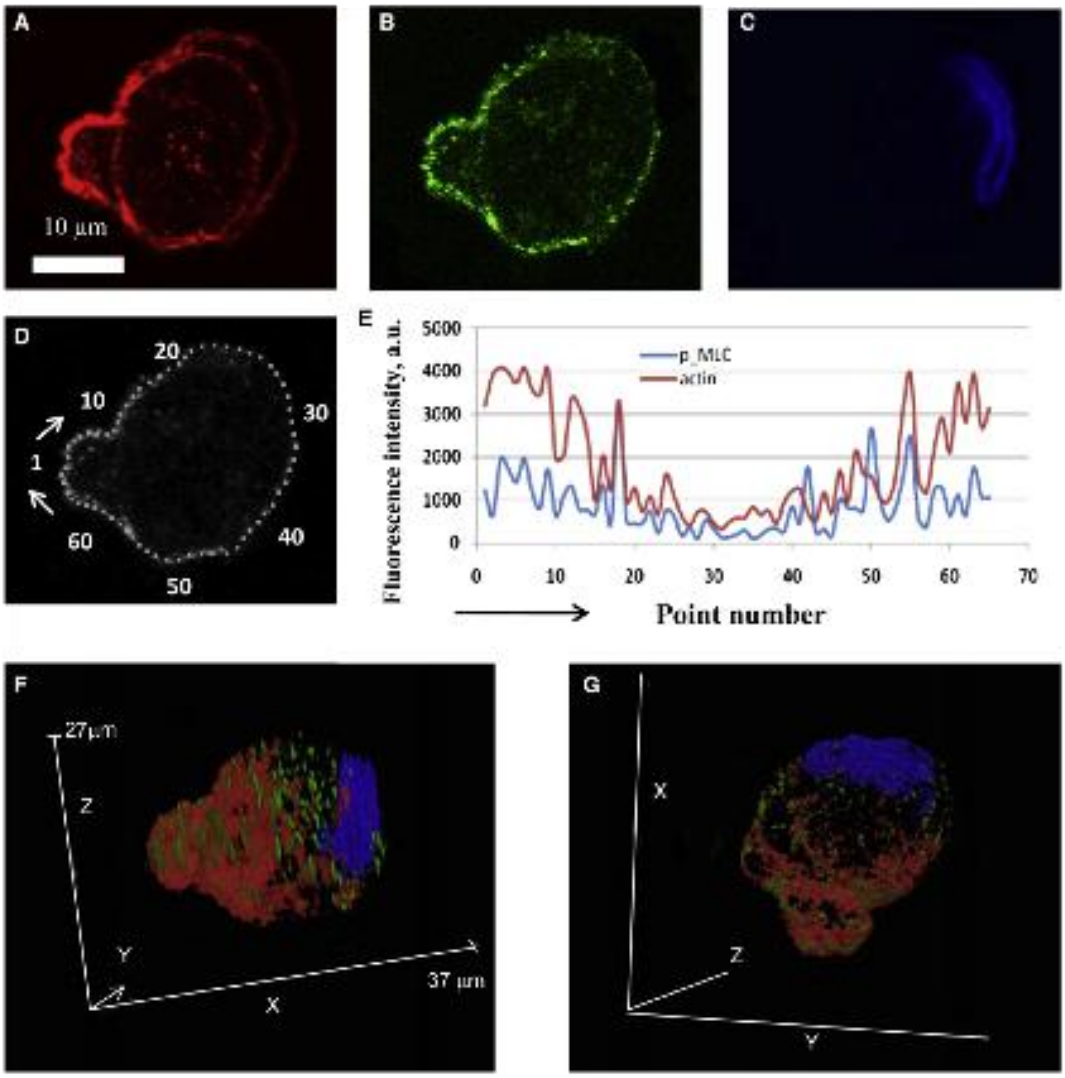
A
10 µm
B
C
D
20
10
30
1
60
40
50
E
Fluorescence intensity, a.u.
5000
4000
3000
2000
1000
0
p_MLC
actin
0
10
20
30
40
50
60
70
Point number
F
27µm
Z
Y
X
37 µm
G
X
Z
Y

Discussion

We previously described the morphological oscillations of spreading cells whose microtubules had been depolymerized (Pletjushkina et al., 2001), and built computational models able to produce oscillations (Kapustina et al., 2008; Weinreb et al., 2006). Our further coarse-grained modeling revealed two competing pathways in which different elements, calcium or RhoA, could play a dominant role in producing oscillations (Weinreb et al., 2009). In this study, we performed a biochemical investigation to distinguish between these pathways and to begin characterization of the regulatory system that underlies the oscillatory behavior. We demonstrate that calcium fluxes from endoplasmic reticulum stores and from the extracellular medium do not significantly affect the ability of cells to oscillate. We found that RhoA activation is necessary but that, other than through microtubule depolymerization, global activation of either RhoA or myosin light chain (MLC) does not induce oscillations. We also characterized the dynamic structure of the oscillating cells showing that these cells are dynamically polarized in terms of their morphology, f-actin and phosphorylated myosin light chain. Concomitantly, the nucleus is moved throughout the cell, and, in the process, undergoes major deformations. We propose that the dynamic cortex observed during oscillations is due to spatiotemporal regulation of RhoA.

Previous work: It is important and interesting to compare and contrast our expanded study of cell oscillations with previous work mainly on suspended cells. Paluch et al. (Paluch et al., 2005) investigated suspended fibroblasts and lymphoblasts

whose microtubules had been depolymerized. In contrast to the present study, in these cells, oscillations appear to be driven by breaks in the actomyosin cortex which allow the remainder of the contractile cortex to push cytoplasm toward the ruptured region, thus forming a large bleb-like structure. Similar to our findings (this paper and (Pletjushkina, 2001)), oscillations were dependent on the actomyosin cytoskeleton and ROCK activity. Salbreux et al. (Salbreux et al., 2007) studied shape oscillations in suspended mouse fibroblasts without microtubule depolymerization. Inhibitor/activator studies showed that these oscillations are also dependent on a contractile actomyosin cytoskeleton with ROCK involvement. However, their work showed that suspended cell oscillations are dependent on calcium, in contrast to the studies reported here on attached cells. These similarities suggest that, in addition to elucidating the structure and mechanochemistry of the cortex, coupling the cell mechanics to the regulatory biochemistry will be important in achieving a detailed understanding of the oscillations in various contexts.

Role of Calcium. The idea that calcium flux could regulate cortical oscillations came from known examples in which changes in intracellular calcium drive periodic contractility: skeletal muscle, cardiomyocytes, and frustrated phagocytosis in macrophages (Berchtold et al., 2000; Katz and Repke, 1966; Kruskal and Maxfield, 1987). In smooth muscle cells, calcium is known to be the predominant regulator with Rho GTPases playing a secondary role in the regulation of contractility (Somlyo and Somlyo, 2003). Further, in migrating neutrophils, tail retraction, which must occur regularly, has been shown to be calcium dependent

(Marks and Maxfield, 1990). In keratocytes this calcium mediated contraction was found to be due to an influx through stretch-activated calcium channels (SACs) (Lee et al., 1999). We therefore proposed (Kapustina et al., 2008; Pletjushkina et al., 2001; Weinreb et al., 2006) that calcium influx from stretch activated calcium channels could be responsible for propagating cortical oscillations in spreading cells. In this view, the negative feedback needed for oscillations comes from increased myosin activity due to local calcium influx that induces a contraction of the actomyosin cortex, thereby closing the SAC channels in that region of the membrane.

We tested this hypothesis by deliberately manipulating calcium. The results from these experiments indicate that our previous hypothesis is not correct: the oscillatory phenotype persists in the absence of extracellular calcium and when SERCA pumps are blocked, demonstrating that fluxes of calcium are not a central player in the oscillatory process. In fact, it was recently discovered that lateral oscillations in keratocytes are also independent of calcium flux (Barnhart et al., 2010). Our previous $[Ca^{2+}]_i$ imaging results (Pletjushkina et al., 2001) were based on a single channel probe, fluo-4, in confocal sections. In light of the substantial periodic excursions of the nucleus and the fact that the nucleus preferentially takes up fluo-4 (Chen et al., 2009), the movements of the nucleus in and out of the confocal section were most likely mistakenly interpreted as a periodic variation in $[Ca^{2+}]_i$.

RhoA regulation. Since $[Ca^{2+}]_i$ does not appear to govern oscillatory behavior, the other known regulator of MLC-phosphorylation, RhoA, is likely to play a significant role in cell oscillations. Rho has a multifaceted role in regulating motile

phenomena. Recent biosensor studies show that RhoA activity displays a complex spatio-temporal pattern of regulation in migrating cells (Machacek et al., 2009; Pertz et al., 2006). Ren et al. investigated the time course of Rho activity during cell spreading and found that in fibroblasts spreading on fibronectin, RhoA activity decreased until about 20 minutes after spreading, and then increased to above the levels found in suspended cells (Ren et al., 1999).

RhoA activates Rho kinase (ROCK) which directly phosphorylates myosin light chain and myosin phosphatasev (Amano et al., 1996; Kimura et al., 1996). ROCK phosphorylation of myosin phosphatase inhibits this enzyme. Therefore, both effects promote a higher level of phosphorylated myosin light chain to increase contractility. Indeed, the dual phosphorylation capacity of ROCK on myosin light chain is thought to provide a stronger stimulus to contractility than the calcium-pathway mediated myosin light chain kinase (Ikebe, 1989; Ueda et al., 2002). In addition, Rho stimulates reformation of the cortex by activating mDia1 (Watanabe et al., 1999) which promotes actin polymerization. We found that RhoA and ROCK were both essential to the propagation of oscillations, but that global activation of RhoA alone did not induce oscillations. Further we found that directly inhibiting MLC phosphatase, which increases global MLC phosphorylation, decreased the percentage of oscillating cells. These results support a model in which spatiotemporal regulation of RhoA in turn provides spatiotemporal regulation of cortical contractility and reconstruction that drives cytoplasmic flows in oscillating cells.

How might Rho regulate oscillatory behavior? We postulate that thinning on one side of the cell leads to an increase in active Rho, which in turn leads to rebuilding of the thinned cortex (via Rho activated formins, such as mDia1) and an increase in cortical contractility through MLC phosphorylation. After some time delay (which will depend on the chemical kinetics of the reactions involved and/or the fluid dynamics of the moving cytosol/cortex and nucleus (Mitchison, 2008), this contractile cortex pushes the cytoplasm and nucleus to another region of the cell, thinning the cortex in that region and initiating another oscillation cycle. This working hypothesis is supported by our imaging data showing differential localization of the contractile cortex during the oscillatory cycle. Moreover, given that RhoA is known to modulate both cortical network formation and contractility, an examination of RhoA with a biosensor capable of capturing spatiotemporal changes in its activity is imperative, and we have begun this investigation in oscillating cells.

Hypothetical pathway dynamic cortex regulation of RhoA: One possible scenario for how RhoA might be regulated by a dynamically polarized cortex follows. In suspended cells and in cells lacking an intact actin cytoskeleton, p190RhoGAP, which converts RhoA back to its inactive form, appears to be neither active nor membrane localized (Mammoto et al., 2007). Rather, this GAP is bound by cytoplasmic filamin. By contrast, in spread cells with an intact cortex, filamin is cleaved by cortex localized calpain and p190RhoGAP becomes localized to the membrane where it is phosphorylated and becomes active. It is plausible that the main regulator of oscillations is a RhoGAP, which is shuttled between the membrane

where it locally inhibits RhoA activation and the cytoplasm where it is bound by filamin, thereby resulting in enhanced RhoA activation at the membrane.

This work raises a number of interesting questions. For example, why does microtubule depolymerization cause the percentage of oscillating cells and the oscillation amplitude to increase? A number of factors may be at play: it is known that removing intact microtubules results in a more deformable cell body, a necessary component of these oscillations (Wang et al., 1993); microtubule depolymerization could also produce non-uniform activation of RhoA, in the process breaking a symmetry and setting up conditions for oscillations; another possibility is that an overshoot in RhoA activation in one part of the cell induces excess contractility that assists in breaking the actin network in preparation for the next expansion in that area. In the case of oscillations in cells in which microtubules have not been depolymerized, it is possible that cells respond to contractile force by some degree of microtubule buckling, as has been predicted (Volokh et al., 2000). In addition to activating myosin-based contractility, RhoA activation also regulates actin polymerization via formins. The question arises as to whether de novo synthesis of the actin network occurs on a time scale compatible with the oscillation period. Also, because Rho family proteins often influence one another, it is likely that other family members are involved but their role remains to be elucidated. More generally, it will be important to ask how the actin rearrangements observed in morphological oscillations are related to those found in cell division and/or cell migration. Finally, do the extreme nuclear displacements and deformations confer features of the

oscillatory phenotype in addition to those observed in enucleated suspension cells (Paluch et al., 2005)?

Clearly, both coarse-grained and fine-grained models of complex cellular phenomena must be informed by experiment. Indeed, this study provides a case in point. Whereas incomplete experimentation previously led to both ODE and CMAP models that could account for the oscillatory phenotype, they were based on a key role for intracellular calcium regulating myosin light chain kinase and thus contractility. By contrast, our current more detailed experiments led us to conclude that calcium mediated contractility plays a subordinate role to that of Rho-induced contractility. Therefore, this work provides a concrete experimental basis to appropriately modify our previous coarse and fine-grained models.

CHAPTER 3

DYNAMIC MECHANOTRANSDUCTION OF THE ACTIN CORTEX DRIVES PROTRUSIONS IN ROUNDED CELLS

Introduction

As cells decrease their area of attachment and adopt rounder morphologies, F-actin is remodeled from integrin-dependent, relatively flat networks to the contractile cortex located at the cell periphery. In vivo environments consist of various materials and 3-dimensional topographies. Cells migrating under such conditions exhibit substantially more cortical actin and myosin II contractility dependence than those on planar surfaces (Doyle et al., 2009; Friedl and Wolf, 2010). However, the mechanisms by which the cortex dynamically regulates cell body protrusions are not known. Here we show that cortical actin density waves that co-localize with RhoA activity drive large-scale periodic protrusions of the cell body. We provide evidence that these waves are driven by a positive feedback loop from myosin II to GEFH1 activation, which occurs at the cortex and is independent of extracellular force-mediated integrin signaling. Our results reveal that intracellular force transduction within the cortex can produce dynamically regulated protrusions as well as function as a signaling substitute for extracellular force transduction.

Fibroblast and epithelial cells exhibit increased cortical actin when migrating in non-planar environments (Doyle et al., 2009). To investigate the mechanochemical properties of the actomyosin cortex, we detached fibroblasts and epithelial cells from the substrate and observed the periodic cell body protrusions that occur upon cell rounding (Costigliola et al. 2010; Paluch et al., 2005). Using confocal microscopy of cells expressing Lifeact-GFP (Riedl et al., 2008) to visualize F-actin, we found that actin waves travel the circumference of the cell during periodic protrusions (Fig. 3.1 A). These waves are driven by myosin II activity and reflect changes in actin density due to regions of contractility rather than large-scale changes in actin polymerization (see Ch. 3). Phosphorylated myosin II co-localizes with actin during periodic protrusions (Costigliola et al. 2010); therefore, we examined the distribution and regulation of an activator of myosin II contractility, the RhoA GTPase, which is necessary for these protrusions (Costigliola et al. 2010), as well as the regulation of cortical actin during migration (Bhadriraju et al., 2007; Poincloux et al. 2011; Wyckoff et al., 2006) and cell division (Bement et al., 2005).

RhoA activity co-localizes with cortical actin density. We co-imaged RhoA activity and actin distribution, using the RBD-3xGFP construct (Benink and Bement, 2005), which binds to active RhoA, and Lifeact-RFP. We found that RhoA activity also exhibits a travelling wave pattern (Fig. 3.1 B) with continuous co-localization to cortical actin (Fig 3.1 C). We analysed the spatiotemporal correlation of actin and RhoA activity by defining the cortical region as a band at the cell periphery encompassing the outer 20% of the cell area and employing the angular coordinate, θ,

to specify position along the band (Fig. 3.1 D). Plotting the cross-correlation in space and time revealed continuous co-localization; that is, the cross-correlation was strongest when comparing RhoA and actin at the same point within the band for all successive images (Fig. 3.1 E). These images were acquired with a line scan frequency on the millisecond timescale, indicating that with this temporal and spatial resolution (see Methods), there is no evidence of actin or RhoA distributions preceding the other. Fig 3.1 F shows the time averaged cross-correlation for each cell, all of which demonstrate a positive cross-correlation at θ=0. The continual co-localization of RhoA activity and actin demonstrates that RhoA activity is both regulated at the cortex and exhibits greatest activity at the densest and most contractile region of the cortex.

Fig 3.1 RhoA activity and actin density co-localize throughout the protrusion cycle. CHO cells were co-transfected, 24 h before being detached from the substrate, with lifeact-RFP, to label filamentous actin (A), and RBD-3xGFP, to detect RhoA activity (B). (C) Overlay of (A) and (B) demonstrates co-localization of actin and RhoA activity in the cortex. Scale bar is 5 μm. (D) Actin and RhoA activity spatial cross-correlation analysis for each cell was calculated for the cortex region (defined as a band at the cell margin encompassing the outer 20% of the cell area). θ is the angular coordinate as defined by radii from the center of the cell area to the cell periphery (see Methods for details). (E) The spatial cross-correlation of actin and RhoA activity for all angular and time coordinates (30 frames) are plotted for a single cell. (F) For each cell, the spatial cross-correlation was time averaged and plotted by coordinate, n=10 cells. Swiss 3T3 cells also exhibit RhoA activity co-localized with actin. [Richard Allen wrote the analysis program for the results shown in Fig 3.1D-F, as described in Methods].

Fig 3.1

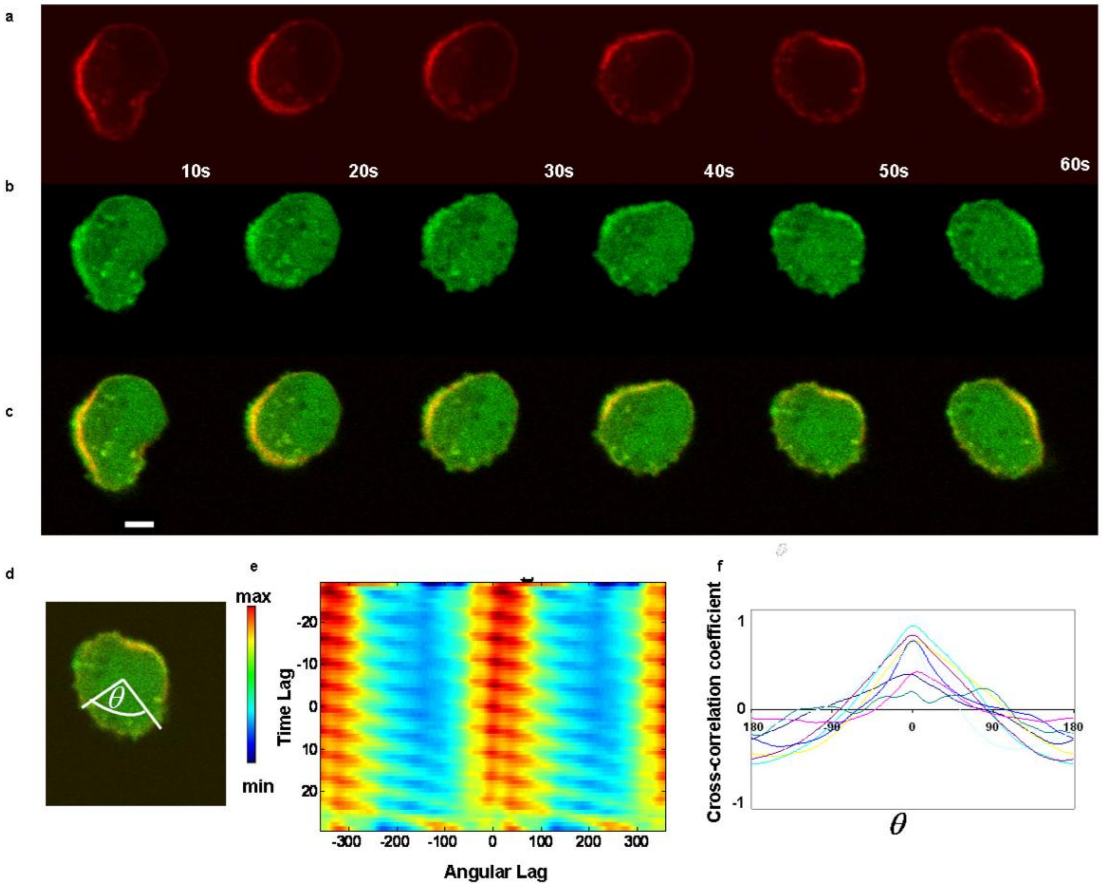
a
b
c
10s
20s
30s
40s
50s
60s
d
e
max
min
Time Lag
-20
-10
0
10
20
-300
-200
-100
0
100
200
300
Angular Lag
f
Cross-correlation coefficient
1
0
-1
180
90
0
90
180
θ

RhoA molecule distribution is polarized. To further investigate the regulation of RhoA activity at the cortex, we sought to determine whether the dense region of activity resulted from local activation of the RhoA molecule and/or distribution of active molecules to the site of polarization. To determine the molecular distribution, we used the RhoA biosensor (Pertz et al., 2006) with a single fluorphore excitation. We found that the biosensor distribution was similar to that of RhoA activity (Fig. 3.2 A) and co-localized with the actin cortex (Fig. 3.2 B,C). Quantification of the cortex to cytoplasm intensities of molecular position gives a two-fold higher intensity at the cortex than within the cytoplasm (n=12 cells, mean cortex/cytoplasm ratio = 2.25 ± 0.9). We found that during periodic protrusions, the biosensor was excluded from the nucleus. The RhoA molecular distribution was strongly anti-correlated with the nuclear position (Fig. 3.2 D). This is similar to observations of uropods in amoeboid breast cancer cells which demonstrate that the nucleus opposes the densest cortical actin structure during migration (Poincloux et al.). Fig. 3.2D shows the spatial correlation in a single frame (time=0) and when the RhoA biosensor position is shifted in time relative to the original nuclear position; this result demonstrates that the anti-correlation during periodic protrusions is remarkably maintained over time. Both the RhoA molecular (Fig. 3.2 A) and RhoA activity (Fig. 3.1 B) distributions exhibited distinctly polarized distributions at the cortex, indicating that a significant proportion of cellular RhoA is distributed to, and is active within, the cortex.

Fig 3.2 RhoA molecule distribution is polarized. (A) the RhoA molecular distribution in a dynamically protruding MEF cell is given by the CFP emission of the RhoA biosensor. Because the periodic protrusion phenotype is diminished when the RhoA biosensor is expressed, this cell has been treated with colcemid to accentuate the phenotype. Scale bar is 10μm. (B) Swiss 3T3 cell, fixed when undergoing periodic protrusions, with the biosensor molecular distribution in green and the F-actin distribution, as labeled by rhodamine phalloidin, in red. (C) Line scan analysis of (B). (D) Spatial cross-correlation of the RhoA molecule maximum fluorescence intensity and the center of the nuclear area, in which the RhoA maximum is shifted over time relative to a reference nuclear position (see Methods for details), n=6 CHO cells. [Richard Allen wrote the analysis program for Fig 3.2D].

Fig 3.2

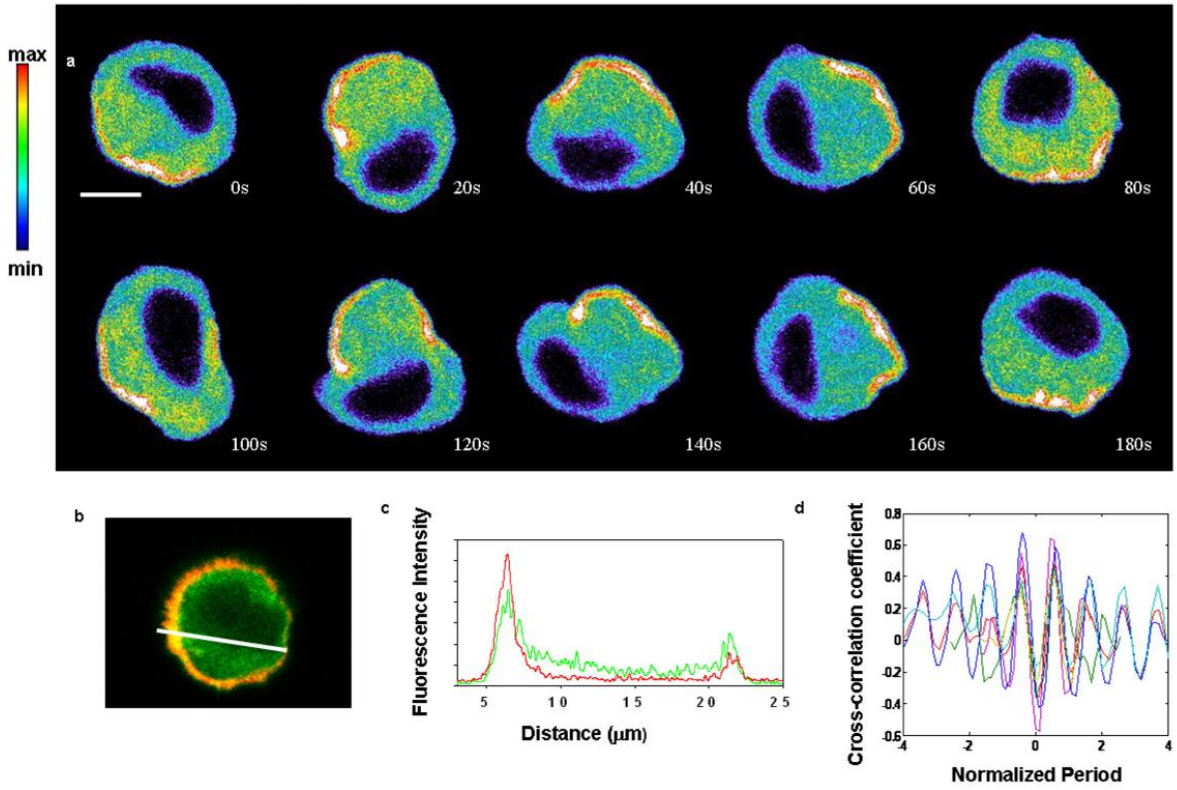
max
min
a
0s
20s
40s
60s
80s
100s
120s
140s
160s
180s
b
c
Fluorescence Intensity
5
10
15
20
25
Distance (μm)
d
Cross-correlation coefficient
0.8
0.6
0.4
0.2
0
-0.2
-0.4
-0.6
-4
-2
0
2
4
Normalized Period

RhoA is both regulated at the cortex during cortical density waves and, in turn, regulates the continuous contractility that drives the waves (Costigliola et al. 2010). It has been shown that positive feedback loops stabilize oscillatory systems(Kim et al., 2010) such as this one. Previous studies have left open the question as to how RhoA might be regulated by cytoskeletal tension at the cortex (Alcaraz et al., 2011; Bershadsky et al., 1996; Birkenfeld et al., 2007; Ren et al., 1999). Here, we test the hypothesis that a positive feedback loop, from RhoA→ROCK→myosin II→RhoA, is active at the cortex and drives cortical density waves.

A myosin II to GEFH1 positive feedback. To investigate which factors could be linking RhoA activation with myosin II contractility, we next investigated several GEFs, or guanine nucleotide exchange factors that determine RhoA molecule position and activity. GEFH1 has been shown to determine cortical actin distribution of RhoA in the latter stages of cytokinesis as well as immediately following mitosis (Birkenfeld et al., 2007), a time in which we also observe periodic protrusions (data not shown). Further, GEFH1 is released from microtubules (MT) and activated upon their depolymerisation (Krendel et al., 2002), a condition under which we observe an increase in the amplitude and propensity of periodic protrusions (Costigliola et al. 2010). MT structure upon cell rounding is visibly distinct from that seen in spread cells (Fig 3.3 A), suggesting that polymers are re-distributed and possibly broken or depolymerized in response to the shape changes that occur. Therefore, we

investigated GEFH1 as a candidate for regulation of RhoA activity at the cortex. We found that GEFH1 undergoes a significant redistribution to cortical actin upon cell detachment from the substrate (Fig. 3.3 B vs. F). Per our hypothesis that a positive feedback between myosin II-based contractility and RhoA activation may be driving cortical density waves, we investigated the distribution of GEFH1-GFP upon inhibition of contractility with the myosin II ATPase inhibitor, blebbistatin (Kovacs et al., 2004). GEFH1 colocalization with cortical actin decreased upon inhibition of myosin II activity: based on whole cell line scan analysis, 35% fewer cells exhibited any correlation to actin upon addition of blebbistatin (n=12 cells without blebbistatin, n=15 cells with blebbistatin, correlation p value <0.0001). See Fig. 3.3 B,D, and C,E, for representative distributions of GEFH1-GFP with and without blebbistatin, and Fig. 3.3 G,H for representative line scans at the cortex.

Fig 3.3 GEFH1 activity and localization is myosin II dependent. (A) Live imaging of tubulin-RFP expressed in a rounded CHO cell. (B-F) GEFH1-GFP expressing cells were fixed and stained with rhodamine phalloidin to visualize actin. (B) GEFH1-GFP in a rounded CHO cell. (C) GEFH1-GFP in a rounded CHO cell in the presence of 5μM blebbistatin. (D) GEFH1-GFP expressed in a spread CHO cell (top panel) and stained for F-actin (red; middle panel). Bottom panel: merged image. (E,F) Overlay of (B and C respectively) with rhodamine phalloidin staining. Bars=5 μm. (G,H) Representative line scan analysis at the cortical region of E and F(white lines), respectively, with actin in red and GEFH1-GFP in black. (I,J) Active GEF-H1, LARG, and p115 were sedimented with GSTRhoAG17A and analysed by western blotting from CHO cells grown on standard culture dishes (I) and from suspended CHO cells (J). 5μM Blebbistatin was added for 2 min in each case (n=4). In each case, total GEF is assayed in the left panel while active GEF is assayed in the right panel. (K,L) CHO cells were transfected for 48 h with control siRNA or siRNA targeting LARG and GEFH1 and co-transfected with Alexa Fluor Red Fluorescent Oligo. Cells were suspended in serum free media containing 200μM RGD peptide and imaged on glass coverslips. In K, only transfected cells exhibiting periodic protrusions were analysed. See Methods for details, n=34 (control siRNA), 11 (GEFH1 knockdown), and 11 cells (LARG knockdown) respectively, *$P<0.01$). (L) Western blots showing knock downs of GEFH1 and LARG with the control siRNA on the left in each blot. γ-tubulin was blotted for as a loading control. [Christophe Guilluy performed the pull-downs and Western blots for the Fig 3.3 I and J.]

Fig 3.3

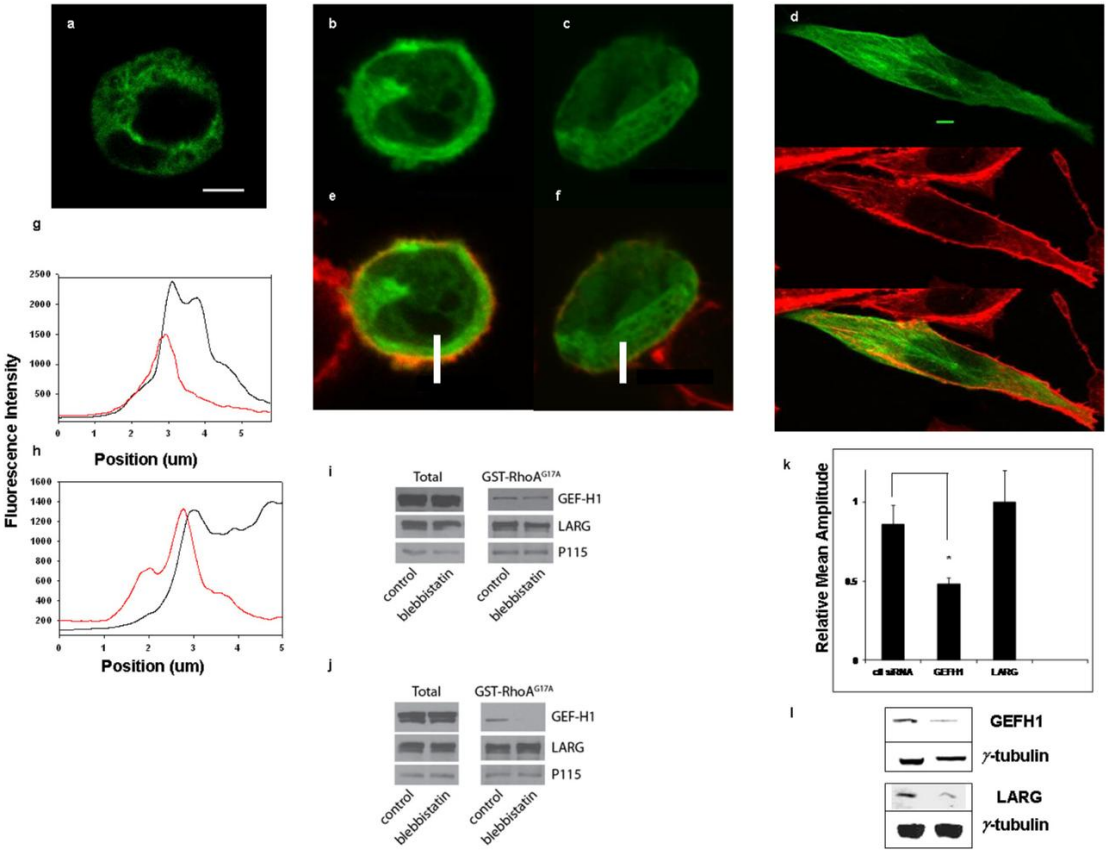
a
b
c
d
e
f
g
Fluorescence Intensity
Position (um)
h
Position (um)
i
Total
GST-RhoA^{G17A}
GEF-H1
LARG
P115
control
blebbistatin
control
blebbistatin
j
Total
GST-RhoA^{G17A}
GEF-H1
LARG
P115
control
blebbistatin
control
blebbistatin
k
Relative Mean Amplitude
GEFH1
LARG
l
GEFH1
γ-tubulin
LARG
γ-tubulin

The fact that GEFH1-GFP redistribution to the cortex depended on myosin II activity was interesting given that GEFH1 distribution to focal adhesions was also found to be dependent on myosin II activity(Kuo et al. 2011). Further, GEFH1 and another GEF, LARG, were activated in response to integrin-mediated force application on the apical surface of spread cells (Guilluy et al. 2011), a process which requires myosin II mediated cell "stiffening." These observations suggest the existence of a positive feedback loop from myosin II-based contractility to GEFH1 and/or LARG activity during extracellular force-mediated integrin signaling. We confirmed this positive feedback by examining the effects of myosin II activity on the activities of GEFH1, LARG, and the GEF p115. We measured GEF activity through the RhoAG17A mutant pull-down (Garcia-Mata et al. 2006) in spread cells with and without 5 μM blebbistatin. We found that with blebbistatin inhibition of myosin II activity, GEFH1 and LARG activities decreased (Fig. 3.3 I), while p115 activity remained constant, consistent with a positive feedback from GEFH1 and LARG to myosin II activity in spread cells.

To compare cortex-mediated with extracellular force-mediated activation of these GEFs, we applied this assay to cells in suspension. We again measured GEFH1, LARG and p115 activities using the RhoAG17A mutant pull-down (Garcia-Mata et al., 2006) assay in suspended cells. GEFH1 activity depended highly on myosin II activity in suspended cells (Fig. 3.3 J). By contrast, LARG and p115, which have been shown to be essential for focal adhesion function (Dubash et al., 2007), did not depend on myosin II activity in suspended cells. This result provides

further evidence for a positive feedback loop from myosin II-based contractility to GEFH1 to RhoA activation to myosin II-based contractility in the cortex of suspended cells.

In order to examine the role of the force-activated GEFs GEFH1 and LARG specifically in cortical wave regulation, we used siRNA interference to knock down expression of these GEFs (Fig. 3.3 L), and assayed periodic protrusions in suspended cells. We suspended siRNA treated cells in serum free media and 200μM arginine-glycine-aspartic acid (RGD) peptide to block integrin engagement(Ruoslahti, 1996) during imaging. Because the density waves anti-correlate strongly with periodic cell protrusions (see Fig. 3.2 D), we used phase-contrast imaging of periodic cell protrusions as a measure of cortical wave regulation. Phase contrast imaging provides a less invasive measurement than fluorescence and allows for study of a more representative cell population(Costigliola et al. 2010). We found that GEFH1 knock down significantly decreased the amplitude of suspended cell protrusions, whereas LARG had no effect (Fig. 3.3 K). This result demonstrates that GEFH1 plays an important role in regulating cortical density waves.

Cortical mechanotransduction. Based on this evidence, we suggest that a positive feedback loop exists in the cortex, wherein, the travelling contractility we observe sustains further propagation of cortical density waves. GEFH1 activates RhoA, which in turn activates myosin II via Rho-kinase and MLC-phosphatase. This positive feedback exists in both the spread and rounded cell states (Fig. 3.3 I,J). In the spread state, extracellular force application to integrins induces downstream

signalling and force transduction via focal adhesion proteins to the actin network (Fig. 3.4 A,B). In the suspended cell state, the cortex itself transduces the mechanochemical signal independently of extracellular force mediated integrin signalling (Fig. 3.4 C,D). We propose that the positive feedback loop from myosin II contractility to GEFH1 facilitates continual wave propagation around the cortex (Fig 3.4 C). Because of the dynamic regulation of contractility that we observe, it is likely that this loop operates at the leading edge of the travelling wave (arrow in Fig. 3.4 C). However, some form of negative feedback is also needed to sustain these waves; it may be that a cortex-distributed RhoA GTPase activating protein (GAP) deactivates RhoA activity at the trailing edge of the wave.

Fig 3.4 Schematic for how the myosi-II to GEFH1 positive feedback could occur in spread and rounded cells. (A,B) A positive feedback between GEFH1 and LARG activation and myosin II contractility has been implicated in extracellular force-mediated integrin signaling (actin network is shown in dark blue, plasma membrane in light blue, and focal adhesion signaling proteins and integrins are in red). Here we confirm this positive feedback. (C) Cortex density waves (high density in red with the remaining cortex in blue) exhibit dynamic mechanochemical signaling independently of extracellular force-mediated integrin signaling. (D) We hypothesize that, within the cortex, GEFH1 locally activates RhoA, which stimulates phosphorylation of myosin II, leading to localized contractility and local strain on the cortex. This then activates GEFH1 in the direction of the traveling wave and drives periodic protrusions.

Fig 3.4

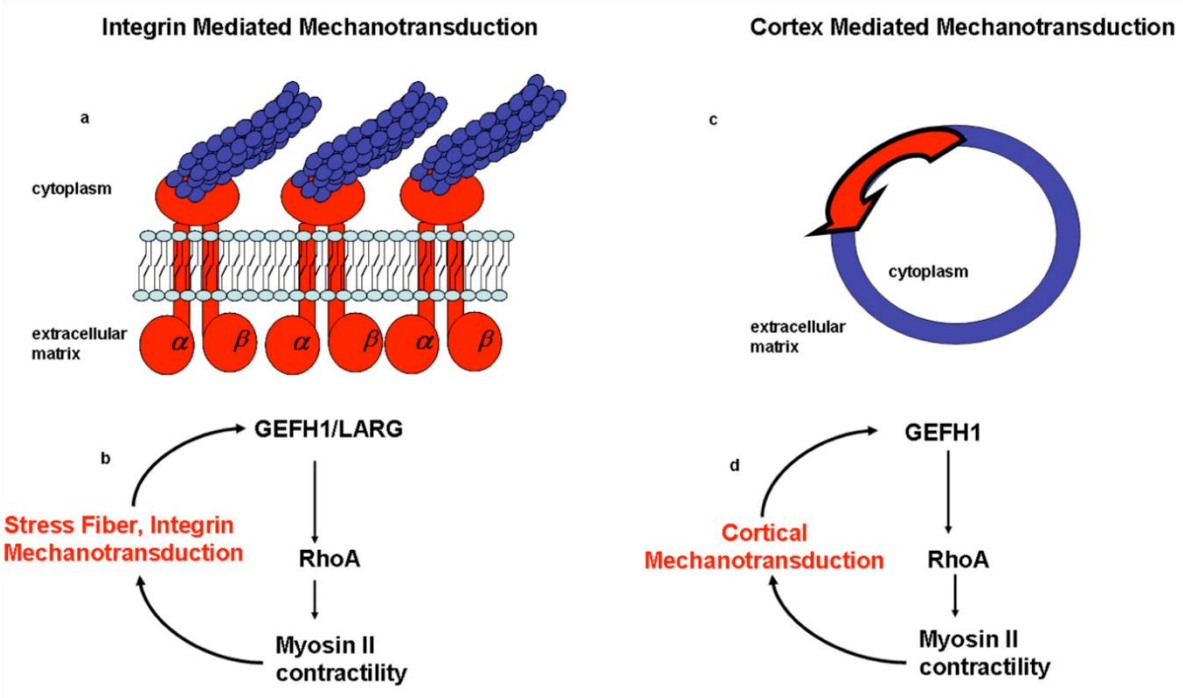
Integrin Mediated Mechanotransduction
a
cytoplasm
extracellular matrix
α
β
α
β
α
β
b
GEFH1/LARG
Stress Fiber, Integrin Mechanotransduction
RhoA
Myosin II contractility
Cortex Mediated Mechanotransduction
c
cytoplasm
extracellular matrix
d
GEFH1
Cortical Mechanotransduction
RhoA
Myosin II contractility

We have demonstrated that a RhoA driven, cortex-specific mechanotransduction drives periodic protrusions in rounded fibroblast and epithelial cells. It is likely that this signalling pathway plays a role in regulating protrusions during migration as well. RhoA has been shown to regulate cortex-driven amoeboid cancer cell movement (Friedl and Alexander, 2011; Pankova et al. 2010) as well as 3D fibrillar migration of fibroblast and endothelial cells, which contain both uni-axial stress fibers and substantial cortical actin (Doyle et al., 2009; Pankov et al., 2005). Cells migrating in 3D environments must navigate materials of varied composition and pore size (Friedl and Wolf, 2010); however, the dynamic regulation of protrusions in these contexts is largely unexplored. Here we demonstrate that myosin II activation of RhoA driven cortical actin waves dynamically regulates periodic protrusions of the cell cortex independently of extracellular-force mediated signalling.

Materials and Methods

Cell Culture and Reagents. Swiss 3T3 and Mouse Embryonic Fibroblasts (MEF) cells were grown in DMEM (Gibco) and CHO cells were grown in DMEM/F12 and DMEM (Gibco), both with 10% FBS (Biowhittaker-Lonza), 5mM Pen-strep and 4mm L-glutamine (Sigma). Colcemid, Y-27632, blebbistatin, and RGD peptide were purchased from Sigma.

Antibodies. For Figure 4.3 L, antibodies were as follows: anti-alpha tubulin and anti-GEFH1 were purchased from abcam, anti-gamma tubulin was purchased from Sigma, and anti-LARG was purchased from Santa Cruz. For Figure 4.3 I and J, antibodies were as described previously(Garcia-Mata et al., 2006) except that anti-GEFH1 was from Bethyl Laboratories.

Immunofluorescence and Transfections. One day prior to transfection, cells were plated on Mat-tek 35 mm glass dishes. For DNA transfections, Swiss 3T3 and CHO cells were transfected using Lipofectamine with Plus reagent (Invitrogen) and imaged 24 hours after transfection. RBD-3xGFP11 was a gift from Bill Bement. Lifeact-RFP5 and tubulin-RFP were gifts from Jim Bear. The RhoA biosensor has been described previously(Pertz et al., 2006). For siRNA transfections, CHO cells were transfected using Lipofectamine RNAimax reagent (Invitrogen)and imaged 48 hours after transfection. A 1:10 dilution of Block-iT Alexa Fluor Red Fluorescent Oligo (Invitrogen) was used to determine transfected cells during imaging. Control siRNA was from Santa Cruz Biotechnology (sc-37007), GEFH1 siRNA (GGAATCCCTCATTGACGAAGAGGTAATCT) EHU092941, and LARG siRNA

(GGAUUAGAAUCUCCCUUAA, UUAAGGGAGAUUUCUAAUCC) were from Sigma.

Imaging. To detach cells from the substrate, the dishes were washed with PBS (Gibco) and then incubated with 1x Trypsin-EDTA (Gibco) while on the microscope in an ambient chamber of 37 C and 5% CO2 for one minute. Trypsin was then removed and media was added back to the dish. Phase contrast imaging and epifluorescence were performed on an Olympus IX-81 with a 20x lens. Confocal imaging was done on an inverted Olympus FV-1000 using a UPLFL 40x oil lens with a 1.3 numerical aperture. All images were 512 x 512 resolution with a pixel acquisition time of 0.5 pixels/μs. Images with more than one wavelength excitation were obtained through sequential line scans and each line of the confocal image was processed with a 3x Kalman filter. Images were acquired every 10s. Confocal sections were 2.0 μm thick or less. For CFP acquisition, the emission range was 460-500nm. For YFP acquisition, the emission range was 515-615nm. For GFP acquisition, the emission range was 480-515nm. For RFP acquisition, the emission range was 600-680nm.

Image analysis. Analysis of the protrusion amplitude was described previously(Costigliola et al.). The cortex to cytoplasm ratio for the RhoA biosensor distribution was calculated by dividing the mean value of a region of interest at the cortex by two separate cytoplasmic regions of interest (ROIs were $1\mu m^2$). Line scans for GEFH1-GFP and rhodamine phalloidin correlation were across the whole cell and

crossing the region of maximum phalloidin intensity. Line correlation values were calculated using Sigma Plot software.

The correlation analyses shown in Figures 1 and 2 were performed using custom Matlab routines developed by Richard Allen. The following description is written by Richard Allen. First the cells were defined using the Otsu's method for thresholding(Otsu, 1979). From this the centroid of each cell was located. Using the centroid as the origin of a local coordinate system, the fluorescence intensity was transformed into polar coordinates:

$$I(r,\theta) = I\left(\left[r\cos(\theta)\right],\left[r\sin(\theta)\right]\right) \qquad (1)$$

where the square brackets indicate rounding to the nearest integer. Note that if the original coordinate system consists of $m \times n$ grid points, the number of grid points in polar coordinates is $r_N \times 360$ where

$$r_N = \sqrt{\left(\frac{m}{2}\right)^2 + \left(\frac{n}{2}\right)^2}\ , \qquad (1)$$

hence the radial coordinate r takes integer values in the range $[1, \ldots, R_N]$.

The position of the nucleus and peak RhoA intensity were defined in the following manner. If $R = [1, \ldots, R_N]$ and $\theta = [1, \ldots 360]$, then define $c \subset R \times \theta$ as the set of points within the cell as defined by our thresholding method. Next define $r_M(\theta)$ as the maximum value or r for a given θ (i.e., $r_M(\theta) = \max[r|\theta]$) and write

$$f_i^k(\theta) = \frac{1}{[(k-i).r_M(\theta)]+1} \sum_{r=[i.r_M(\theta)]}^{[k.r_M(\theta)]} I(r,\theta) \quad (1)$$

where $f_i^k(\theta)$ is the average intensity for a given angle in a predefined intra-cellular annulus with outer and inner radii given by $[k \cdot r_M(\theta)]$ and $[i \cdot r_M(\theta)]$, respectively, and $k < i < 1$. Since the nucleus was located approximately in the center of the cell and the biosensor was excluded from the nucleus, we defined the angular position of the nucleus, θ_N, as $\left[f_i^k(\theta) \right]_N = \min f_i^k(\theta)$ with $i = 1/r_M$ and $k = 0.5$. The maximum peripheral RhoA intensity, θ_R, is given by $\left[f_i^k(\theta) \right]_R = \max f_i^k(\theta)$ this time taking $i = 0.8$ and $k = 1$. In both cases the $f_i^k(\theta)$ was smoothed using cubic splines prior to ascertaining the positional information. By analyzing every frame in this manner we tracked both these positions as functions of time. The cross-correlation was calculated as $\langle \cos(\theta_N) \cdot \cos(\theta_R) \rangle$. Note that for some frames, the oscillation was only observable in the y-projection, rather than the x-projection (due to the time between frames being approximately half the period of the oscillation). In these cases the y-projection was used to quantify the cross-correlation. The resulting cross-correlation was normalized by the period of the oscillation.

We similarly used Eq. (1) to quantify the co-localization of RhoA and liveact with $i = 0.8$ and $k = 1$. This defines the intensity of RhoA and liveact around the periphery of the cell; $f_R(\theta)$ and $f_L(\theta)$, respectively. To show that the peak RhoA intensity co-localized with the peak liveact intensity we calculated the periodic cross-correlation $(f_R \cdot f_L)(\theta)$.

Statistical analysis: Statistical differences between two groups of data were analysed with a two-tailed unpaired Students t-test.

CHAPTER 4

DISCUSSION AND FUTURE STUDIES

In this work I have shown that the RhoA pathway, rather than the calcium signaling pathway, is the primary regulator of periodic protrusions. I have developed criteria for measuring these protrusions and I have found that they occur spontaneously upon cell rounding in fibroblast and epithelial cells. These protrusions occur in the absence of integrin-mediated signaling and thus demonstrate a novel form of cortical mechanotransduction. The dynamic contractility we observe in the suspended cell is regulated by RhoA as well as its upstream activator GEFH1. GEFH1 activity and distribution, in turn, are dependent on myosin II activity, demonstrating the role of a positive feedback in driving periodic protrusions. GEFH1 direct binding to active myosin II was shown to have no effect on RhoA activity, while Rac and Cdc42 activities decreased upon this interaction (Lee et al., 2010) . I hypothesize that myosin II contractility activates GEFH1 indirectly via cortical strain.

I speculate that within the cortex, signaling pathways similar to those acting downstream of force mediated integrin signaling are present. Our collaborators (Guilluy et al., 2011) found that GEFH1 was activated in response to force via a FAK-Ras-ERK pathway in cells plated on planar substrates. Others have observed that FAK activity and recruitment to focal adhesions is myosin II dependent

(Pasapera et al., 2010). It is possible that the FAK pathway is part of the positive feedback loop from myosin II to GEFH1 activity that we observe. Testing the involvement of this pathway is a clear next step in this work. FAK inhibitors could be used to test their effects on GEFH1 activity in suspended cells, as well as their effect on periodic protrusions.

To test the existence of a positive feedback, the myosin light chain phosphatase inhibitor, calyculin, could be added to suspended cells to test whether this increased GEFH1 activity via enhancement of myosin II activity. Another option to pursue would be to use migrating cells, which are not subject to the confines of a periodic system. Examination of cancer cell uropods for cortical density folds and for dependence on the myosin II to GEFH1 positive feedback could be a promising avenue to pursue in conjunction with the periodic protrusive phenotype. Because discrete focal contacts do not form in the absence of substrate contact (which I confirmed by expressing paxillin-GFP in rounded cells, data not shown), I propose that mechanosensitive focal adhesion associated proteins transduce mechanical signals within the cortex of rounded cells via an alternate structural organization. It may be that the accordion-like folding of the cortex-membrane interface during cortical actin waves provides a unique environment in which focal adhesion proteins are activated without focal adhesion formation. Research into how this structural organization could regulate downstream signaling would be a valuable direction of further study.

REFERENCES

Aggeler, J., Ward, J., Blackie, L.M., Barcellos-Hoff, M.H., Streuli, C.H., and Bissell, M.J. (1991). Cytodifferentiation of mouse mammary epithelial cells cultured on a reconstituted basement membrane reveals striking similarities to development in vivo. Journal of cell science *99 (Pt 2)*, 407-417.

Alcaraz, J., Mori, H., Ghajar, C.M., Brownfield, D., Galgoczy, R., and Bissell, M.J. (2011). Collective epithelial cell invasion overcomes mechanical barriers of collagenous extracellular matrix by a narrow tube-like geometry and MMP14-dependent local softening. Integrative biology : quantitative biosciences from nano to macro *3*, 1153-1166.

Amano, M., Ito, M., Kimura, K., Fukata, Y., Chihara, K., Nakano, T., Matsuura, Y., and Kaibuchi, K. (1996). Phosphorylation and activation of myosin by Rho-associated kinase (Rho-kinase). The Journal of biological chemistry *271*, 20246-20249.

Arthur, W.T., and Burridge, K. (2001). RhoA inactivation by p190RhoGAP regulates cell spreading and migration by promoting membrane protrusion and polarity. Mol Biol Cell *12*, 2711-2720.

Barnhart, E.L., Allen, G.M., Julicher, F., and Theriot, J.A. (2010). Bipedal locomotion in crawling cells. Biophysical journal *98*, 933-942.

Bement, W.M., Benink, H.A., and von Dassow, G. (2005). A microtubule-dependent zone of active RhoA during cleavage plane specification. J Cell Biol *170*, 91-101.

Benink, H.A., and Bement, W.M. (2005). Concentric zones of active RhoA and Cdc42 around single cell wounds. J Cell Biol *168*, 429-439.

Berchtold, M.W., Brinkmeier, H., and Muntener, M. (2000). Calcium ion in skeletal muscle: its crucial role for muscle function, plasticity, and disease. Physiol Rev *80*, 1215-1265.

Bershadsky, A., Chausovsky, A., Becker, E., Lyubimova, A., and Geiger, B. (1996). Involvement of microtubules in the control of adhesion-dependent signal transduction. Curr Biol *6*, 1279-1289.

Bhadriraju, K., Yang, M., Alom Ruiz, S., Pirone, D., Tan, J., and Chen, C.S. (2007). Activation of ROCK by RhoA is regulated by cell adhesion, shape, and cytoskeletal tension. Exp Cell Res *313*, 3616-3623.

Birkenfeld, J., Nalbant, P., Bohl, B.P., Pertz, O., Hahn, K.M., and Bokoch, G.M. (2007). GEF-H1 modulates localized RhoA activation during cytokinesis under the control of mitotic kinases. Dev Cell *12*, 699-712.

Bissell, M.J., and Barcellos-Hoff, M.H. (1987). The influence of extracellular matrix on gene expression: is structure the message? Journal of cell science Supplement *8*, 327-343.

Blaser, H., Reichman-Fried, M., Castanon, I., Dumstrei, K., Marlow, F.L., Kawakami, K., Solnica-Krezel, L., Heisenberg, C.P., and Raz, E. (2006). Migration of zebrafish primordial germ cells: a role for myosin contraction and cytoplasmic flow. Developmental cell *11*, 613-627.

Bornens, M., Paintrand, M., and Celati, C. (1989). The cortical microfilament system of lymphoblasts displays a periodic oscillatory activity in the absence of microtubules: implications for cell polarity. The Journal of cell biology *109*, 1071-1083.

Burridge, K., and Wennerberg, K. (2004). Rho and Rac take center stage. Cell *116*, 167-179.

Cai, Y., Rossier, O., Gauthier, N.C., Biais, N., Fardin, M.A., Zhang, X., Miller, L.W., Ladoux, B., Cornish, V.W., and Sheetz, M.P. (2010). Cytoskeletal coherence requires myosin-IIA contractility. Journal of cell science *123*, 413-423.

Carreno, S., Kouranti, I., Glusman, E.S., Fuller, M.T., Echard, A., and Payre, F. (2008). Moesin and its activating kinase Slik are required for cortical stability and microtubule organization in mitotic cells. The Journal of cell biology *180*, 739-746.

Charras, G., and Paluch, E. (2008). Blebs lead the way: how to migrate without lamellipodia. Nature reviews Molecular cell biology *9*, 730-736.

Charras, G.T., Coughlin, M., Mitchison, T.J., and Mahadevan, L. (2008). Life and times of a cellular bleb. Biophysical journal *94*, 1836-1853.

Charras, G.T., Hu, C.K., Coughlin, M., and Mitchison, T.J. (2006). Reassembly of contractile actin cortex in cell blebs. The Journal of cell biology *175*, 477-490.

Chen, Z., Li, Z., Peng, G., Chen, X., Yin, W., Kotlikoff, M.I., Yuan, Z.Q., and Ji, G. (2009). Extracellular ATP-induced nuclear Ca2+ transient is mediated by inositol 1,4,5-trisphosphate receptors in mouse pancreatic beta-cells. Biochem Biophys Res Commun *382*, 381-384.

Costigliola, N., Kapustina, M.T., Weinreb, G.E., Monteith, A., Rajfur, Z., Elston, T.C., and Jacobson, K. RhoA regulates calcium-independent periodic contractions of the cell cortex. Biophys J *99*, 1053-1063.

Cukierman, E., Pankov, R., and Yamada, K.M. (2002). Cell interactions with three-dimensional matrices. Curr Opin Cell Biol *14*, 633-639.

Cunningham, C.C., Gorlin, J.B., Kwiatkowski, D.J., Hartwig, J.H., Janmey, P.A., Byers, H.R., and Stossel, T.P. (1992). Actin-binding protein requirement for cortical stability and efficient locomotion. Science *255*, 325-327.

Diz-Munoz, A., Krieg, M., Bergert, M., Ibarlucea-Benitez, I., Muller, D.J., Paluch, E., and Heisenberg, C.P. (2010). Control of directed cell migration in vivo by membrane-to-cortex attachment. PLoS biology *8*, e1000544.

Dobereiner, H.G., Dubin-Thaler, B.J., Giannone, G., and Sheetz, M.P. (2005). Force sensing and generation in cell phases: analyses of complex functions. J Appl Physiol *98*, 1542-1546.

Doherty, G.J., and McMahon, H.T. (2008). Mediation, modulation, and consequences of membrane-cytoskeleton interactions. Annual review of biophysics *37*, 65-95.

Doyle, A.D., Wang, F.W., Matsumoto, K., and Yamada, K.M. (2009). One-dimensional topography underlies three-dimensional fibrillar cell migration. J Cell Biol *184*, 481-490.

Dubash, A.D., Wennerberg, K., Garcia-Mata, R., Menold, M.M., Arthur, W.T., and Burridge, K. (2007). A novel role for Lsc/p115 RhoGEF and LARG in regulating RhoA activity downstream of adhesion to fibronectin. J Cell Sci *120*, 3989-3998.

Even-Ram, S., and Yamada, K.M. (2005). Cell migration in 3D matrix. Curr Opin Cell Biol *17*, 524-532.

Fackler, O.T., and Grosse, R. (2008). Cell motility through plasma membrane blebbing. The Journal of cell biology *181*, 879-884.

Farsad, K., and De Camilli, P. (2003). Mechanisms of membrane deformation. Current opinion in cell biology *15*, 372-381.

Friedl, P., and Alexander, S. (2011). Cancer invasion and the microenvironment: plasticity and reciprocity. Cell *147*, 992-1009.

Friedl, P., and Wolf, K. (2010). Plasticity of cell migration: a multiscale tuning model. J Cell Biol *188*, 11-19.

Garcia-Mata, R., Wennerberg, K., Arthur, W.T., Noren, N.K., Ellerbroek, S.M., and Burridge, K. (2006). Analysis of activated GAPs and GEFs in cell lysates. Methods Enzymol *406*, 425-437.

Gardel, M.L., Schneider, I.C., Aratyn-Schaus, Y., and Waterman, C.M. (2010). Mechanical integration of actin and adhesion dynamics in cell migration. Annual review of cell and developmental biology *26*, 315-333.

Geiger, B., Bershadsky, A., Pankov, R., and Yamada, K.M. (2001). Transmembrane crosstalk between the extracellular matrix--cytoskeleton crosstalk. Nature reviews Molecular cell biology *2*, 793-805.

Guilluy, C., Swaminathan, V., Garcia-Mata, R., O'Brien, E.T., Superfine, R., and Burridge, K. The Rho GEFs LARG and GEF-H1 regulate the mechanical response to force on integrins. Nat Cell Biol *13*, 722-727.

Hakkinen, K.M., Harunaga, J.S., Doyle, A.D., and Yamada, K.M. (2011). Direct comparisons of the morphology, migration, cell adhesions, and actin cytoskeleton of fibroblasts in four different three-dimensional extracellular matrices. Tissue engineering Part A *17*, 713-724.

Hamill, O.P., and Martinac, B. (2001). Molecular basis of mechanotransduction in living cells. Physiological reviews *81*, 685-740.

Hoffman, B.D., Grashoff, C., and Schwartz, M.A. (2011). Dynamic molecular processes mediate cellular mechanotransduction. Nature *475*, 316-323.

Huttenlocher, A., and Horwitz, A.R. (2011). Integrins in cell migration. Cold Spring Harbor perspectives in biology *3*, a005074.

Ikebe, M. (1989). Phosphorylation of a second site for myosin light chain kinase on platelet myosin. Biochemistry *28*, 8750-8755.

Ikenoya, M., Hidaka, H., Hosoya, T., Suzuki, M., Yamamoto, N., and Sasaki, Y. (2002). Inhibition of rho-kinase-induced myristoylated alanine-rich C kinase substrate (MARCKS) phosphorylation in human neuronal cells by H-1152, a novel and specific Rho-kinase inhibitor. J Neurochem *81*, 9-16.

Jain, S.S. (2005). Inadvertent filtering bleb following sutureless cataract surgery. Indian journal of ophthalmology *53*, 196-198.

Kanchanawong, P., Shtengel, G., Pasapera, A.M., Ramko, E.B., Davidson, M.W., Hess, H.F., and Waterman, C.M. (2010). Nanoscale architecture of integrin-based cell adhesions. Nature *468*, 580-584.

Kapustina, M., Weinreb, G.E., Costigliola, N., Rajfur, Z., Jacobson, K., and Elston, T.C. (2008). Mechanical and biochemical modeling of cortical oscillations in spreading cells. Biophys J *94*, 4605-4620.

Katsumi, A., Milanini, J., Kiosses, W.B., del Pozo, M.A., Kaunas, R., Chien, S., Hahn, K.M., and Schwartz, M.A. (2002). Effects of cell tension on the small GTPase Rac. The Journal of cell biology *158*, 153-164.

Katz, A.M., and Repke, D.I. (1966). Control of myocardial contraction: the sensitivity of cardiac actomyosin to calcium ion. Science *152*, 1242-1243.

Kim, J.R., Shin, D., Jung, S.H., Heslop-Harrison, P., and Cho, K.H. (2010). A design principle underlying the synchronization of oscillations in cellular systems. J Cell Sci *123*, 537-543.

Kimura, K., Ito, M., Amano, M., Chihara, K., Fukata, Y., Nakafuku, M., Yamamori, B., Feng, J., Nakano, T., Okawa, K., *et al.* (1996). Regulation of myosin phosphatase by Rho and Rho-associated kinase (Rho-kinase). Science *273*, 245-248.

Kovacs, M., Toth, J., Hetenyi, C., Malnasi-Csizmadia, A., and Sellers, J.R. (2004). Mechanism of blebbistatin inhibition of myosin II. J Biol Chem *279*, 35557-35563.

Krendel, M., Zenke, F.T., and Bokoch, G.M. (2002). Nucleotide exchange factor GEF-H1 mediates cross-talk between microtubules and the actin cytoskeleton. Nat Cell Biol *4*, 294-301.

Kruskal, B.A., and Maxfield, F.R. (1987). Cytosolic free calcium increases before and oscillates during frustrated phagocytosis in macrophages. J Cell Biol *105*, 2685-2693.

Kuo, J.C., Han, X., Hsiao, C.T., Yates, J.R., 3rd, and Waterman, C.M. Analysis of the myosin-II-responsive focal adhesion proteome reveals a role for beta-Pix in negative regulation of focal adhesion maturation. Nat Cell Biol *13*, 383-393.

Lee, C.S., Choi, C.K., Shin, E.Y., Schwartz, M.A., and Kim, E.G. (2010). Myosin II directly binds and inhibits Dbl family guanine nucleotide exchange factors: a possible link to Rho family GTPases. J Cell Biol *190*, 663-674.

Lee, J., Ishihara, A., Oxford, G., Johnson, B., and Jacobson, K. (1999). Regulation of cell movement is mediated by stretch-activated calcium channels. Nature *400*, 382-386.

Legant, W.R., Pathak, A., Yang, M.T., Deshpande, V.S., McMeeking, R.M., and Chen, C.S. (2009). Microfabricated tissue gauges to measure and manipulate forces

from 3D microtissues. Proceedings of the National Academy of Sciences of the United States of America *106*, 10097-10102.

Lipowsky, R. (1991). The conformation of membranes. Nature *349*, 475-481.
Liu, B.P., Chrzanowska-Wodnicka, M., and Burridge, K. (1998). Microtubule depolymerization induces stress fibers, focal adhesions, and DNA synthesis via the GTP-binding protein Rho. Cell Adhes Commun *5*, 249-255.

Lorentzen, A., Bamber, J., Sadok, A., Elson-Schwab, I., and Marshall, C.J. (2011). An ezrin-rich, rigid uropod-like structure directs movement of amoeboid blebbing cells. Journal of cell science *124*, 1256-1267.

Machacek, M., Hodgson, L., Welch, C., Elliott, H., Pertz, O., Nalbant, P., Abell, A., Johnson, G.L., Hahn, K.M., and Danuser, G. (2009). Coordination of Rho GTPase activities during cell protrusion. Nature *461*, 99-103.

Maddox, A.S., and Burridge, K. (2003). RhoA is required for cortical retraction and rigidity during mitotic cell rounding. J Cell Biol *160*, 255-265.

Mammoto, A., Huang, S., and Ingber, D.E. (2007). Filamin links cell shape and cytoskeletal structure to Rho regulation by controlling accumulation of p190RhoGAP in lipid rafts. J Cell Sci *120*, 456-467.

Marks, P.W., and Maxfield, F.R. (1990). Transient increases in cytosolic free calcium appear to be required for the migration of adherent human neutrophils. J Cell Biol *110*, 43-52.

Nambiar, R., McConnell, R.E., and Tyska, M.J. (2009). Control of cell membrane tension by myosin-I. Proceedings of the National Academy of Sciences of the United States of America *106*, 11972-11977.

Nobes, C.D., and Hall, A. (1995). Rho, rac, and cdc42 GTPases regulate the assembly of multimolecular focal complexes associated with actin stress fibers, lamellipodia, and filopodia. Cell *81*, 53-62.

Nourshargh, S., Hordijk, P.L., and Sixt, M. (2010). Breaching multiple barriers: leukocyte motility through venular walls and the interstitium. Nature reviews Molecular cell biology *11*, 366-378.

Otsu, N. (1979). A Threshold Selection Method from Gray-Level Histograms. IEEE Transactions on Systems, Man, and Cybernetics *Vol. 9*, 62-66.

Paluch, E., Piel, M., Prost, J., Bornens, M., and Sykes, C. (2005). Cortical actomyosin breakage triggers shape oscillations in cells and cell fragments. Biophys J *89*, 724-733.

Pankov, R., Endo, Y., Even-Ram, S., Araki, M., Clark, K., Cukierman, E., Matsumoto, K., and Yamada, K.M. (2005). A Rac switch regulates random versus directionally persistent cell migration. J Cell Biol *170*, 793-802.

Pankova, K., Rosel, D., Novotny, M., and Brabek, J. The molecular mechanisms of transition between mesenchymal and amoeboid invasiveness in tumor cells. Cell Mol Life Sci *67*, 63-71.

Pasapera, A.M., Schneider, I.C., Rericha, E., Schlaepfer, D.D., and Waterman, C.M. (2010). Myosin II activity regulates vinculin recruitment to focal adhesions through FAK-mediated paxillin phosphorylation. The Journal of cell biology *188*, 877-890.

Pertz, O., Hodgson, L., Klemke, R.L., and Hahn, K.M. (2006). Spatiotemporal dynamics of RhoA activity in migrating cells. Nature *440*, 1069-1072.

Pesen, D., and Hoh, J.H. (2005). Micromechanical architecture of the endothelial cell cortex. Biophysical journal *88*, 670-679.

Petrie, R.J., Doyle, A.D., and Yamada, K.M. (2009). Random versus directionally persistent cell migration. Nat Rev Mol Cell Biol *10*, 538-549.

Pletjushkina, O.J., Rajfur, Z., Pomorski, P., Oliver, T.N., Vasiliev, J.M., and Jacobson, K.A. (2001). Induction of cortical oscillations in spreading cells by depolymerization of microtubules. Cell Motil Cytoskeleton *48*, 235-244.

Poincloux, R., Collin, O., Lizarraga, F., Romao, M., Debray, M., Piel, M., and Chavrier, P. Contractility of the cell rear drives invasion of breast tumor cells in 3D Matrigel. Proc Natl Acad Sci U S A *108*, 1943-1948.

Raghavan, S., Shen, C.J., Desai, R.A., Sniadecki, N.J., Nelson, C.M., and Chen, C.S. (2010). Decoupling diffusional from dimensional control of signaling in 3D culture reveals a role for myosin in tubulogenesis. Journal of cell science *123*, 2877-2883.

Ren, X.D., Kiosses, W.B., and Schwartz, M.A. (1999). Regulation of the small GTP-binding protein Rho by cell adhesion and the cytoskeleton. Embo J *18*, 578-585.

Riedl, J., Crevenna, A.H., Kessenbrock, K., Yu, J.H., Neukirchen, D., Bista, M., Bradke, F., Jenne, D., Holak, T.A., Werb, Z., *et al.* (2008). Lifeact: a versatile marker to visualize F-actin. Nat Methods *5*, 605-607.

Riveline, D., Zamir, E., Balaban, N.Q., Schwarz, U.S., Ishizaki, T., Narumiya, S., Kam, Z., Geiger, B., and Bershadsky, A.D. (2001). Focal contacts as mechanosensors: externally applied local mechanical force induces growth of focal contacts by an mDia1-dependent and ROCK-independent mechanism. The Journal of cell biology *153*, 1175-1186.

Rottner, K., Hall, A., and Small, J.V. (1999). Interplay between Rac and Rho in the control of substrate contact dynamics. Current biology : CB *9*, 640-648.
Ruoslahti, E. (1996). RGD and other recognition sequences for integrins. Annu Rev Cell Dev Biol *12*, 697-715.

Sahai, E., and Marshall, C.J. (2003). Differing modes of tumour cell invasion have distinct requirements for Rho/ROCK signalling and extracellular proteolysis. Nature cell biology *5*, 711-719.

Salbreux, G., Joanny, J.F., Prost, J., and Pullarkat, P. (2007). Shape oscillations of non-adhering fibroblast cells. Phys Biol *4*, 268-284.

Sanz-Moreno, V., Gadea, G., Ahn, J., Paterson, H., Marra, P., Pinner, S., Sahai, E., and Marshall, C.J. (2008). Rac activation and inactivation control plasticity of tumor cell movement. Cell *135*, 510-523.

Sheetz, M.P., Sable, J.E., and Dobereiner, H.G. (2006). Continuous membrane-cytoskeleton adhesion requires continuous accommodation to lipid and cytoskeleton dynamics. Annual review of biophysics and biomolecular structure *35*, 417-434.

Somlyo, A.P., and Somlyo, A.V. (2003). Ca2+ sensitivity of smooth muscle and nonmuscle myosin II: modulated by G proteins, kinases, and myosin phosphatase. Physiol Rev *83*, 1325-1358.

Stricker, J., Aratyn-Schaus, Y., Oakes, P.W., and Gardel, M.L. (2011). Spatiotemporal constraints on the force-dependent growth of focal adhesions. Biophysical journal *100*, 2883-2893.

Tickle, C.A., and Trinkaus, J.P. (1973). Changes in surface extensibility of Fundulus deep cells during early development. Journal of cell science *13*, 721-726.

Trinkaus, J.P. (1973). Surface activity and locomotion of Fundulus deep cells during blastula and gastrula stages. Developmental biology *30*, 69-103.

Tsuji, T., Ishizaki, T., Okamoto, M., Higashida, C., Kimura, K., Furuyashiki, T., Arakawa, Y., Birge, R.B., Nakamoto, T., Hirai, H., *et al.* (2002). ROCK and mDia1 antagonize in Rho-dependent Rac activation in Swiss 3T3 fibroblasts. J Cell Biol *157*, 819-830.

Ueda, K., Murata-Hori, M., Tatsuka, M., and Hosoya, H. (2002). Rho-kinase contributes to diphosphorylation of myosin II regulatory light chain in nonmuscle cells. Oncogene *21*, 5852-5860.

Volokh, K.Y., Vilnay, O., and Belsky, M. (2000). Tensegrity architecture explains linear stiffening and predicts softening of living cells. Journal of biomechanics *33*, 1543-1549.

Wang, N., Butler, J.P., and Ingber, D.E. (1993). Mechanotransduction across the cell surface and through the cytoskeleton. Science *260*, 1124-1127.

Watanabe, N., Kato, T., Fujita, A., Ishizaki, T., and Narumiya, S. (1999). Cooperation between mDia1 and ROCK in Rho-induced actin reorganization. Nat Cell Biol *1*, 136-143.

Weinreb, G.E., Elston, T.C., and Jacobson, K. (2006). Causal mapping as a tool to mechanistically interpret phenomena in cell motility: application to cortical oscillations in spreading cells. Cell Motil Cytoskeleton *63*, 523-532.

Weinreb, G.E., Kapustina, M.T., Jacobson, K., and Elston, T.C. (2009). In silico generation of alternative hypotheses using causal mapping (CMAP). PLoS One *4*, e5378.

Wolf, K., and Friedl, P. (2011). Extracellular matrix determinants of proteolytic and non-proteolytic cell migration. Trends in cell biology *21*, 736-744.

Wolfenson, H., Bershadsky, A., Henis, Y.I., and Geiger, B. (2011). Actomyosin-generated tension controls the molecular kinetics of focal adhesions. Journal of cell science *124*, 1425-1432.

Wyckoff, J.B., Pinner, S.E., Gschmeissner, S., Condeelis, J.S., and Sahai, E. (2006). ROCK- and myosin-dependent matrix deformation enables protease-independent tumor-cell invasion in vivo. Curr Biol *16*, 1515-1523.